

POLITECNICO DI TORINO

**MASTER's Degree in
PHYSICS OF COMPLEX SYSTEMS**



MASTER's Degree Thesis

**A TWO-COMPONENT MODEL FOR
PHASE SEPARATION DRIVEN
MOLECULAR SORTING**

Supervisors

Prof. ANDREA GAMBA

Prof. LUCA DALL'ASTA

Candidate

SILVIA VARESCHI

OCTOBER 2022

Summary

Molecular sorting is a highly complex process taking place in eukaryotic cells, in which specific cargo molecules are collected in vesicles and dispatched to appropriate destinations. The first fundamental step of sorting, vesicle formation, is possible through the aggregation, on the membrane, of cargo molecules and a number of different endocytic proteins. The formation of such aggregate promotes membrane bending, leading to the budding and the extraction of a vesicle enriched with the engulfed molecular components.

Recently, a theoretical model of this process was proposed (we will refer to it as “one-component” model), where the following events are described: proteins arrive on a membrane region, diffuse and aggregate into localized enriched domains, that are ultimately extracted after reaching a characteristic size. Under appropriate conditions, the system self-organizes into a driven non-equilibrium stationary state, that is characterized by the coexistence of phase-separated sorting domains with a gas of freely diffusing molecules. In particular it was highlighted the existence of a region of values, in the aggregation parameter g , where the sorting process is most efficient and, therefore, leads to low-density stationary states.

In that prototypical model the aggregation of proteins of a single type was considered, however this is far from the actual biological process. To take more into account the complexity of the phenomenon, this thesis proposes a two-component model (we will refer to it as the “AB” model), in which sorting domains are formed by the aggregation of two species: cargo (“B” species) and auxiliary molecules (“A” species). Cargo can only diffuse laterally once inserted into the membrane. Auxiliary molecules are present in a fixed number and are recycled after each extraction event. Differently from the cargo, auxiliaries are able to shuttle between membrane and cytosol, where their diffusivity is much faster than on the membrane. A contact attractive interaction, (quantified by the aggregation parameter g) is assumed to exist between particles belonging to different species while the interaction between particles of the same species is of excluded volume type, meaning that a domain will need both species to form.

Our investigation aims to answer two questions. The first one asks to understand what is the effect of having a limited pool of auxiliary proteins, which are necessary

to form domains, and how it changes with the aggregation parameter.

The second question arises from an observation on the different dynamics followed by the two species: if we focus on a small region of the membrane for relatively short time scales (shorter than the typical time scale of domain growth and extraction and of cargo insertion) we see that the concentration field of the cargo is locally conserved on the membrane. On the contrary, the fast redistribution mechanism followed by the auxiliaries implies that their concentration field is approximately globally - but not locally - conserved on the membrane. This observation is useful since, according to theories of phase separation processes, systems described by a non-locally-conserved order parameter show a faster coarsening than systems that are described by a locally-conserved one. Because of this, it is reasonable to ask whether the interaction of cargoes with molecules that follow a faster, non-locally-conserved dynamics can be advantageous for the process.

The model proposed in this thesis has been studied numerically, by implementing a Gillespie algorithm and describing the membrane as a square lattice with periodic boundary conditions, coupled to an unstructured cytosol. In order to discern the effect of non-local-conservation of the auxiliaries the algorithm was also implemented for a variant "B'B" model: in this case "A" molecules are substituted by "B'" molecules which differ for being able only to diffuse along the membrane (they cannot shuttle between membrane and cytosol, but still they are present in a finite number and are recycled after each extraction event). The behaviour of the AB and the B'B model was then studied by varying the value of the aggregation factor g and the number of auxiliaries per unit membrane site ($N_{\text{aux}}/N_{\text{sites}}$), starting from an empty membrane initial condition. The AB model was additionally investigated in a regime of faster redistribution of the auxiliaries. A preliminary analysis was also conducted starting from a non-empty membrane.

Results show that, independently from the specific dynamics followed by the auxiliaries, our model is characterized by a rich phenomenology, where the stability of low-density stationary states changes as we vary the number of auxiliaries and the aggregation parameter. This results in a new, sharp transition between a parameter region where sorting occurs under optimal conditions (the existence of such optimal region is reminiscent of the one-component model) and neighboring regions where sorting is disfavoured. Simulations also show the appearance of a parameter region where the stationary state is characterized by peculiar large oscillations in the density, due to the alternation of long "quiescent" periods, where extraction events are rare, and periods where the extraction activity is very intense. Finally, results show that faster shuttling of the auxiliary molecules can increase the efficiency of the sorting process.

This thesis is structured as follows:

- In Chapter 1 an introduction to the biological process is given, with a particular focus on the paradigmatic case of clathrin-mediated-endocytosis

- In Chapter 2 phase separation theory is introduced
- In Chapter 3 the “one-component” model for molecular sorting, already present in literature, is introduced, together with the main results achieved
- Chapter 4 introduces the “AB” and the “B’B’ ” models. The features chosen are discussed.
- In Chapter 5 the numerical method used to study the model is presented
- Finally, in Chapter 6 and 7 results are presented and discussed

Acknowledgements

Table of Contents

1	Molecular sorting	1
1.1	Spatial organization in living cells	1
1.2	Coated vesicles formation: the example of clathrin mediated endo- cytosis	4
2	Phase separation processes	9
2.1	Passive vs active phase separation	9
2.2	Relaxation dynamics	11
2.3	Coarsening and competition between domains	15
2.3.1	Conserved dynamics	15
2.3.2	Non conserved dynamics	17
3	Phase separation in molecular sorting: one-component model	20
4	Phase separation in molecular sorting: introducing a two-component model	25
4.1	AB model	27
4.2	B'B model	28
4.3	Parameter dependence	28
5	Model and Algorithm	30
5.1	Model formalization	30
5.2	Gillespie algorithm	31
5.2.1	Basic ideas	31
5.2.2	Implementation	33
6	Results	38
6.1	Case 1: B'B dynamics	39
6.2	Case 2: AB dynamics	44
6.3	Case 3: fast AB dynamics	48
6.4	Comparison between the three cases	52

6.5	Large oscillations	53
6.6	Comparison with the one-component model	60
6.7	Observed transitions	61
6.8	Dependence on the initial conditions	64
7	Discussion and conclusions	67
	Bibliography	69

Chapter 1

Molecular sorting

“Everything in its right place”
Radiohead, Kid A

1.1 Spatial organization in living cells

Paraphrasing its thermodynamic definition given by Schroedinger, life can be thought as a “**struggle against disorder**”, indeed, differently from inanimate systems, living organisms avoid a rapid decay to the state of maximum entropy and behave in a manner that is apparently purely mechanical, in contrast to thermodynamic, i.e. it is not affected by thermal disorder [1]. Evolution of life thus followed a path that lead organisms to develop strategies to contrast the homogenizing effect of thermal disorder such that, even if the laws of chance still hold, their outcome is different. Among these strategies there are the “invention” of the macro-molecule and the “invention” of the cell, basic unit of life, characterized by a high spatial organization (Fig. 1.1a).

How is this **spatial organization** possible? A paradigm that has become particularly useful and seems quite universal is that of **phase-separation**, that was successfully applied to explain the formation of *non-membrane-bound compartments in the cytosol* (Fig.1.2a) [4],[5], the formation of *transient enriched domains on the cell membrane* (Fig.1.2b) [6],[7],[8],[9],[10]and the *organization of genetic information in the nucleus* (Fig.1.2c, [11]). Interactions driving the phase separation can be direct (e.g. arising from contact interactions) or effective, sustained by positive and negative chemical feedback loops [6, 12].

Eukariotic cells are further organized into functionally distinct, **membrane enclosed compartments** (organelles), each of them enriched in a particular set of molecules. The expression “**molecular sorting**” (or “protein sorting”) refers to the maintenance of the biochemical differences between organelles, that is possible

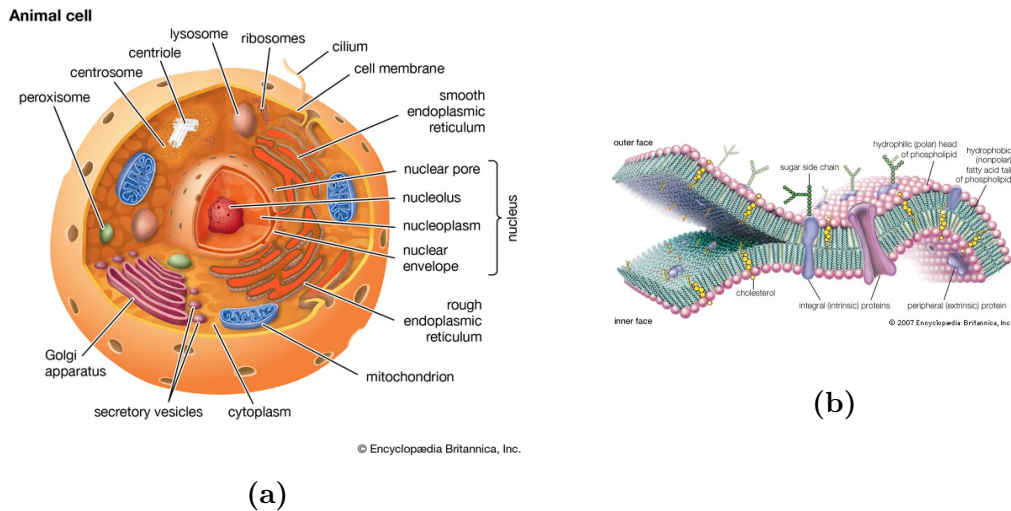


Figure 1.1: (a): schematic organization of a eukariotic cell. From [2]. (b) schematic representation of a cell membrane. From [3].

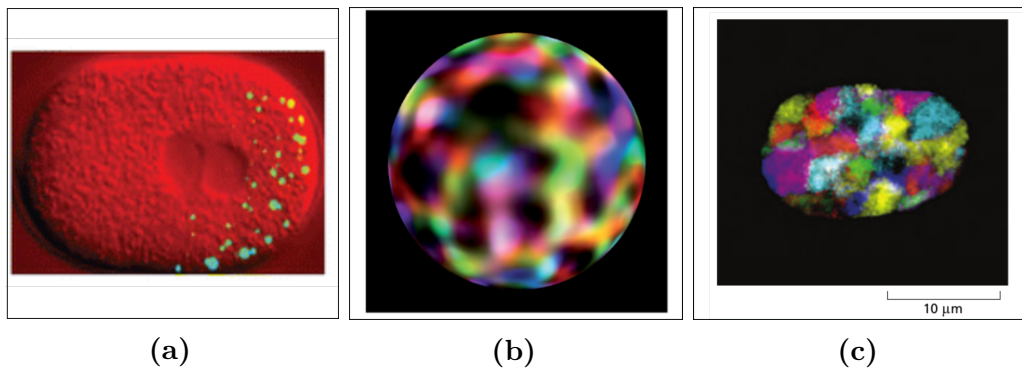


Figure 1.2: (a): P-granules found in the cytosol of *Caenorhabditis elegans*. From [4](b): Transient domains on the plasma membrane of a eukaryotic cell. From [13]. (c): Chromosome territories in the nucleus. From [14].

through a complex intracellular membrane traffic (Fig.1.3a), characterized by the budding of transport vesicles from one compartment and their fusion with the other: as they do so they carry material as cargo from the lumen and membrane of the donor compartment to the lumen and membrane of the target compartment (Fig.1.3b). So, in the case of membrane bound compartments, compartmentalization of molecular species involves a further layer of complexity in that phase separation processes are coupled to membrane mechanics. Phase separation processes are indeed crucial both to identify target membranes and to initiate the process of membrane budding. which is the subject of this thesis.

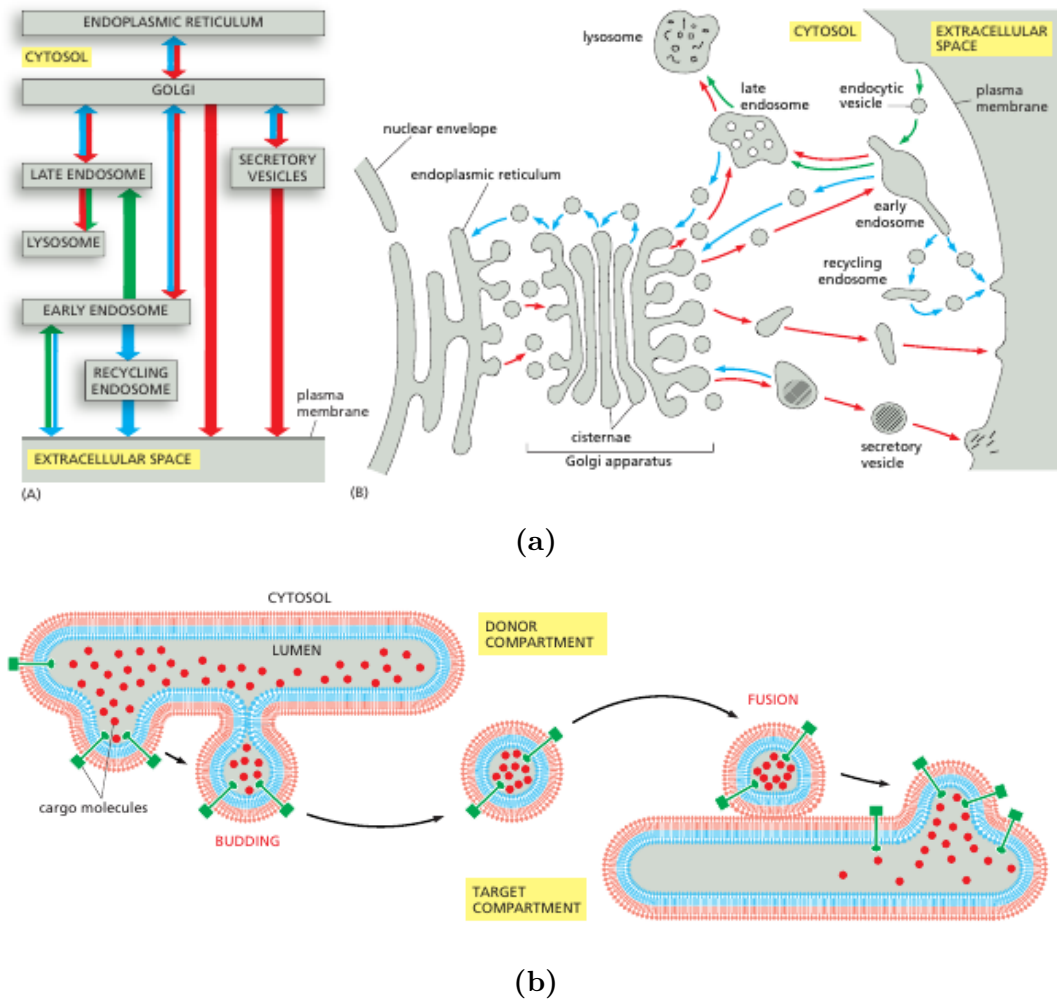


Figure 1.3: (a): "road-map" of intracellular membrane traffic.(b): Budding and fusion of a transport vesicle. Figures from [15]

There are many routes that lead to membrane budding, most of them have in common the fact that transport vesicles bud off as **coated vesicles**. The coat has a double function, reflected in a common two layer structure: an inner layer concentrates specific membrane proteins in specialized patch in order to select the appropriate membrane molecules for transport, an outer layer induces bending of the membrane and shapes the vesicles. A coat is formed by many different types of proteins and different type of coats exist, which are characterized by different molecular species involved: three well characterized coated vesicles are *clathrin-coated vesicles*, *COPI-coated vesicles* and *COPII-coated vesicles*, that take their name from the major component of the coat and are specialized for different

transport steps. However, this list is not exhaustive since there is variety even in these three types. The minimal model I will discuss in the next chapters transcends molecular details, so that the results are likely to be applicable in general to coated vesicles. In the following section I give a more detailed description of *clathrin mediated endocytosis* (the word *endocytosis* refers to the process of vesicle formation) in that clathrin coated vesicles have been the first to be identified, however the process of their formation is quite paradigmatic and conceptually similar to the ones that lead to the formation of other types of coated vesicles.

1.2 Coated vesicles formation: the example of clathrin mediated endocytosis

The process of **clathrin mediated endocytosis** was first described 5 decades ago and, since then, over 50 proteins have been shown to be part of the machinery and characterized in detail. Despite being studied for a long time, since the process is very complex, there are a lot of open questions, mainly related to how all these different components work together in a highly coordinated manner to drive vesicle formation. An interesting review [16] was written recently and in the following I will mainly refer to it as well as [15]. However complex, endocytosis is a conceptually

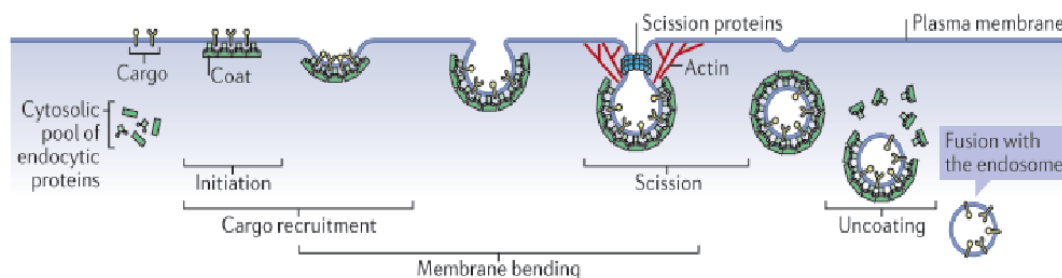


Figure 1.4: steps of clathrin mediated endocytosis. Figure from [16]

fairly simple process that consists of a few sequential and *partially overlapping* steps, that are representend in the cartoon in Fig.1.4:

Initiation : endocytic coat proteins from the cytosol start to cluster on the inner leaflet of the plasma membrane

Continuation : further recruitment of other coat proteins from the cytosolic pool allows the protein coat assembly to continue growing.

Cargo recruitment : cargo molecules are concentrated to the coated region of the plasma membrane.

Membrane bending : the assembling coat transforms the flat plasma membrane into a 'clathrin-coated pit'

Scission : the membrane invagination is constricted and cut, separating the clathrin-coated vesicle from the plasma membrane. Actin polymerization cooperates with the coat and scission proteins to promote membrane shaping.

Uncoating : the endocytic protein machinery disassembles and the nascent cargo-filled vesicle is released and allowed to be trafficked within the cell.

Thus, on the basis of their dynamics, the endocytic proteins can be grouped into functional modules: *coat module*, *actin module*, *scission module*, *uncoating module*. Extensive interactions take place within and between modules to coordinate the assembly and functions.

As it will be discussed in the next chapters, the model studied in this thesis deals with the process of aggregation of cargo and coat proteins, while it does not directly tackle with membrane bending, scission and uncoating. The **coat module** is composed by *clathrin adaptor proteins* (eg. adaptor protein AP2 complex) and by *scaffold proteins* (e.g.: clathrin, Fig.1.5), that interact with the clathrin adaptors and with themselves to cluster the coat components together as well as to induce membrane bending. It is possible to identify an earliest assembling coat that forms a **pioneer module** (Fig. 1.6) , responsible for initiating the endocytic process [16], [17]. Coat assembly is crucial for the **initiation** of the process and defines the

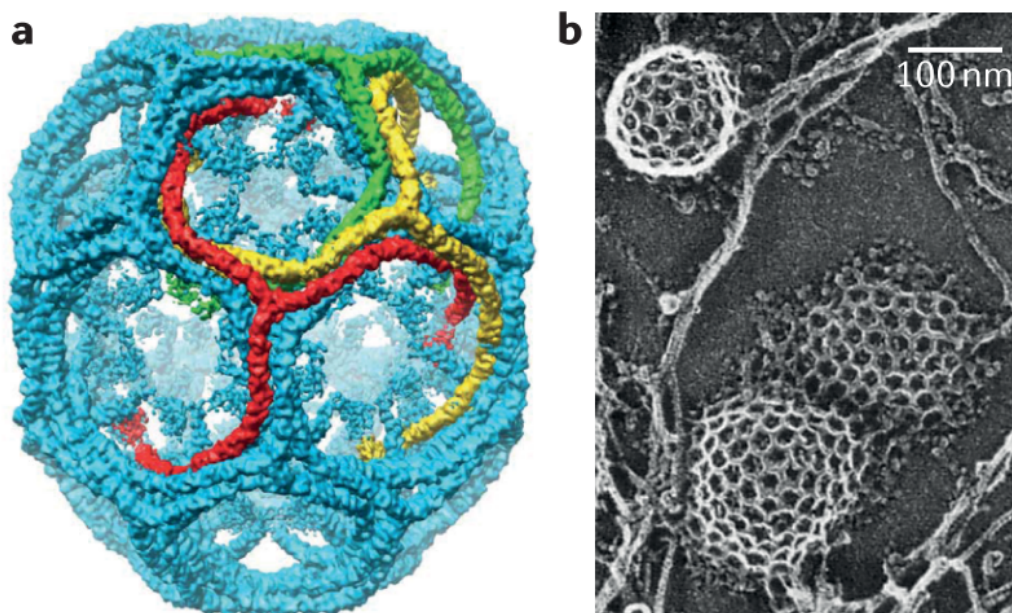


Figure 1.5: Structure of a clathrin coat. Figures adapted respectively from [18] and [19]

position where endocytosis will take place: in some cases endocytic events appear

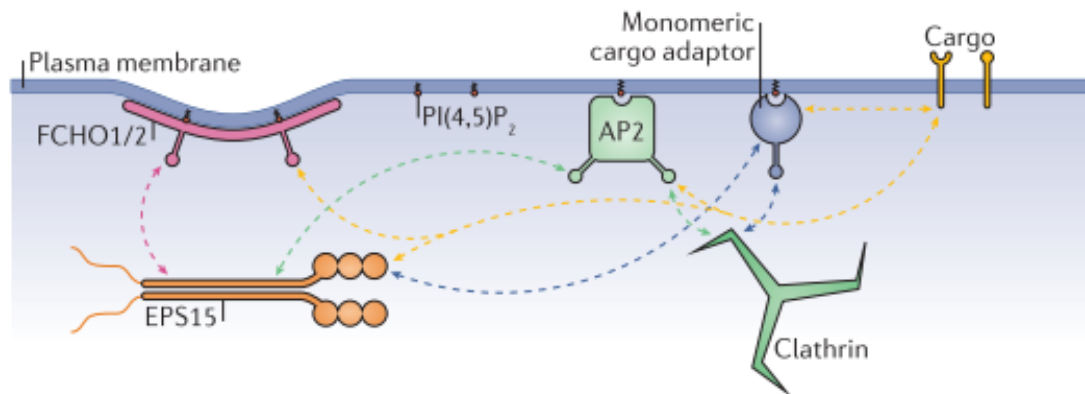


Figure 1.6: Proteins of the pioneer module, which includes the F-BAR domain only protein 1 and 2 complex (FCHO1/2), the adaptor protein AP2 complex, epidermal growth factor receptor substrate 15 (EPS15) and monomeric cargo adaptors. From [16]

to be initiated at random positions but, in many cases, the initiation is clearly spatial non random and this may be due to the existence of plasma membrane domains or regions with endocytosis promoting properties such as the ability to concentrate specific lipids or endocytic cargo proteins.

This stage is also responsible for **cargo loading** (the word "cargo" refers to transmembrane proteins and their extracellular ligands). The basic principle in cargo recruitment is that proteins of the clathrin coat bind to specific sites in the cytosolic part of different transmembrane cargo molecules, so that specific cargoes will be enriched in the forming vesicles and then selectively endocytosed, indeed a large number of clathrin-adaptor proteins (including many of the early arriving coat component) and scaffolds proteins have been shown to directly interact with specific cargoes and function as cargo adaptors for them. Because of this, it is reasonable to think that the cargo molecules may recruit the pioneer proteins to the plasma membrane and increase the likelihood of initiation of an endocytic event. Furthermore, cargo-checkpoint mechanisms have been described, that guarantee vesicles that form are filled with cargo molecules: a possible mechanism is the stabilization of the pit by the presence of cargo, as argued in [20] (see Fig. 1.7) and [21].

The way cargo recruitment is coordinated with coat assembly is highly cooperative since, in addition to binding to cargoes, most adaptors also interact directly with lipids and with other coat proteins, thereby forming a complex network of interactions that can mediate initiation of clathrin coat assembly and its further expansion. An example is the case of AP2 complex that can act to coordinate

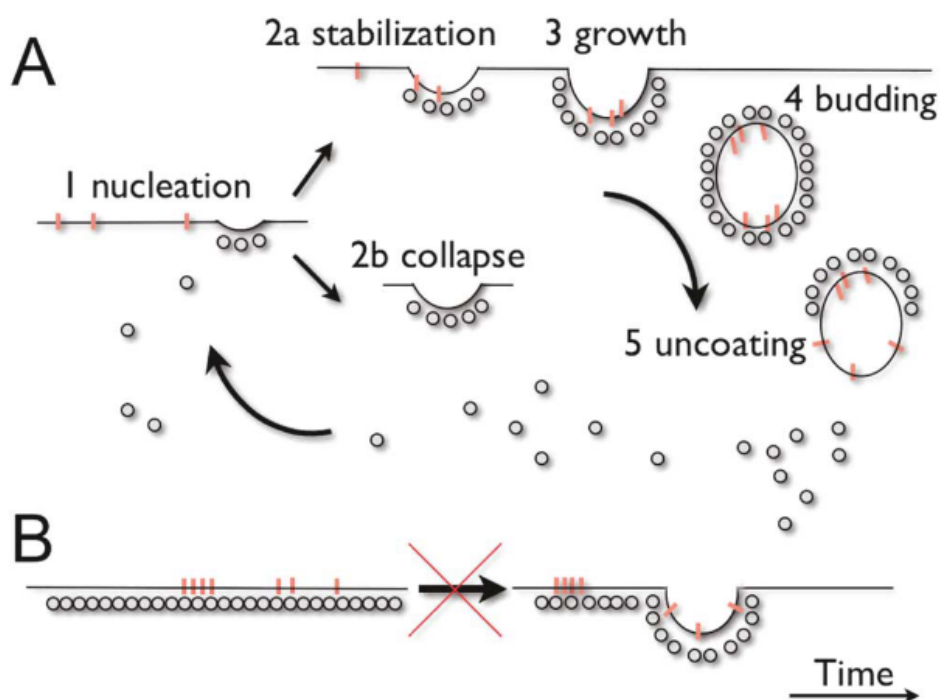


Figure 1.7: Model proposed in [20]: coat formation is characterized by an initial exploratory phase, during which coated pits continue to grow but collapse rapidly if conditions required for coat stabilization are not met. Alternatively the forming coated pit stabilizes, perhaps by cargo capture.

cargo recruitment with coat assembly, thus possibly regulating the initiation and/or maturation of the endocytic coat: binding of AP2 with the phospholipid $PI(4,5)P_2$ is associated with a large conformational change in AP2, that enables binding with clathrin and cargo (Fig.1.8).

So the process of coat formation and vesicle extraction is highly complex and involves many different proteins that interact both directly and through self-enforcing feedback loops. Interestingly, if we focus on the dynamics of molecular factors present on the membrane we can see that the process can be thought as a phase separation: in a regime where vesicle formation occurs we can identify the coexistence of a high density phase of coat proteins and a low density one. Following this viewpoint, recently a minimal model has been proposed [22], [23] and this thesis will proceed in that direction. Because of this, in the next chapter, I first review some classical theories about phase separation.

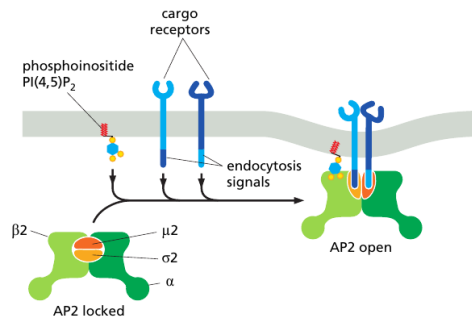


Figure 1.8: Upon interaction with the phosphoinositide PI(4,5)P₂ in the cytosolic leaflet of the plasma membrane, AP2 rearranges so that binding sites for cargo receptors become exposed. When AP2 binds tightly to the membrane, it induces curvature, which favors the binding of additional AP2 complexes in the vicinity. From [15]

Chapter 2

Phase separation processes

*“Because we separate
Like ripples on a blank shore”
Radiohead, Reckoner*

2.1 Passive vs active phase separation

The formation of domains of endocytic molecules (cargo, adaptors, clathrins) can be thought as a phase separation process where the two phases are i) regions with high density of endocytic molecules ii) regions with low density of endocytic molecules; in particular it resembles the phenomenon of precipitation of a solute in a solvent, where the domains are the precipitate. Vesicle scission can be thought as an annihilation reaction that takes place once a sufficient large domain has formed.

In **classical thermodynamic context**, phase separation is a *transient non equilibrium process by which an initially well-mixed equilibrium state transforms to a demixed equilibrium state following an appropriate change of thermodynamic conditions*. Fig.2.1 shows the phase diagram for the behaviour of a binary mixture: in the space of temperature and relative concentration it is possible to identify areas where the system is in a mixed state and areas where demixing takes place.

In the case of **phase separation occurring in biological systems**, everything is complicated by the fact that the system is **active**, i.e. it *exchanges matter with the environment, reactions occur and there are energy consuming mechanisms* that introduce a well defined “arrow”, such that in general detailed balance does not hold. In such active systems the final state may differ from the equilibrium one (if work and energy were not supplied) and it is not so immediate to define a free energy. A possible classification of current theoretical descriptions of inhomogeneous phase separating systems has been recently proposed in [24] and consists in four categories:

1. **Passive systems**: systems where phase equilibria and domain kinetics show

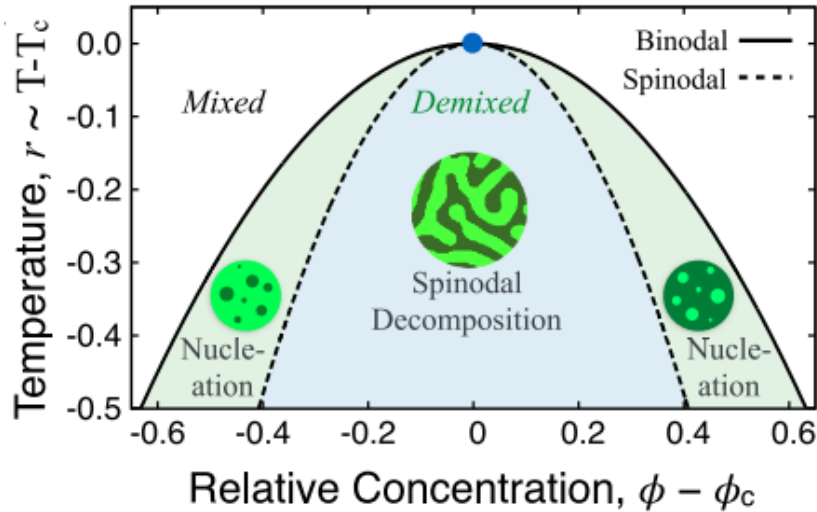


Figure 2.1: Thermodynamics of phase separation. Simple binary phase diagrams showing regions of immiscibility and of mixed phase instability, delimited by binodal and spinodal boundaries, respectively. Critical points are indicated by blue dots. Figure from [24]

no significant deviations from equilibrium thermodynamics

2. **Modulate passive systems:** systems that differ from passive ones only in the addition of space and/or time dependent equilibrium or external parameters
3. **Undriven chemically reactive systems:** systems where chemical kinetics take place but no internal or external energy sources supply work or drive the system. Such mixtures satisfy detailed balance in equilibrium and therefore relax to thermal equilibrium, as far as no special boundary conditions are applied. Domain evolution kinetics may be altered relative to non reactive mixtures, however thermodynamic equilibrium is not affected by the presence of reactions.
4. **Driven chemically reactive systems:** systems where work is supplied through external forces, heat transfer, mass transfer or internal energy sources and can alter thermodynamic stability of phases.

Categories (1) and (2) don't involve explicit treatment of chemical reactions or any other active process; categories (1), (2) and (3) share the common fundamental feature that each is predicated on the existence of a thermodynamic free energy density and a relaxation to local thermal equilibrium. Category (4), instead, is fundamentally different, since i) reaction rates can be dictated by driving forces other than the local chemical potential, ii) detailed balance can be violated and iii) a well defined free energy functional does not exist, rather a nonequilibrium free

energy functional is sought.

Unluckily (or interestingly) our system seems to fall in category (4), since we have a flux of matter and vesicle extraction (Fig.2.2). However, looking at the case of

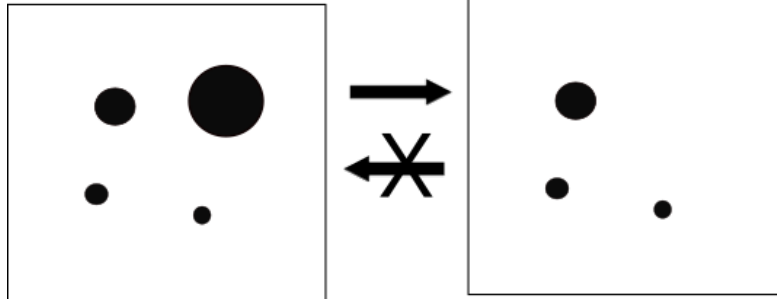


Figure 2.2: Black domains represent portions of the cell enriched with coat proteins. On the left we see the system before an extraction event occurs, on the right the extraction event took place. The extraction event is not reversible because coated vesicles cannot merge following the same pathway. In other words, detailed balance does not hold.

phase separation in passive systems is still instructive since it has been studied for decades and can give interesting hints to the behaviour of the phenomenon.

2.2 Relaxation dynamics

Among the approaches that have been developed in order to describe the transition, a possibility is a phenomenological field theoretic formalism that describes the relaxation dynamics of an order parameter in a energetic landscape. The **order parameter** is defined as a field $\Phi(x, t)$ coming from a coarse-graining of microscopic degrees of freedom on an area that is much larger than the lattice spacing but much smaller than the correlation length. Such theories follow two principles: 1) a system let evolved in contact with a thermal bath should tend to Gibbs equilibrium distributions 2) conservation laws that characterize the microscopic dynamics must still hold at the coarse grained level. The prototype of a **relaxational dynamics** is the behaviour of a brownian particle, described by the Langevin equation:

$$\frac{dv(t)}{dt} = F(t) - \Gamma v(t) + \eta \quad (2.1)$$

where η is a noise term such that $\langle \eta(t) \rangle = 0$ $\langle \eta(t)\eta(t') \rangle = 2D\delta(t - t')$ and the damping coefficient Γ is linked to diffusivity D by Einsteins relation $D = \Gamma K_B T$. Extending this approach to the description of the dynamics of a countinuous degree

of freedom defined in the space it is possible to obtain:

$$\frac{\partial\phi(x,t)}{\partial t} = - \int \Gamma(x-x') \frac{\delta\mathcal{H}[\phi]}{\delta\phi(x',t)} dx' + \eta(x,t) \quad (2.2)$$

where:

- η is such that $\langle\eta(t)\rangle = 0$, $\langle\eta(x,t)\eta(x',t')\rangle = 2D\delta(t-t')\delta(x-x')$
- the action is defined as $\mathcal{S}[\phi] = \beta\mathcal{H}[\phi] = \int dx [\frac{1}{2}(\nabla\phi)^2 + V[\phi]]$
- a useful form for the potential is $V[\phi(x)] = \frac{\mu^2}{2}\phi(x)^2 + \frac{\lambda}{4!}\phi^4 - J(x,t)\phi(x,t)$, describing a double well subject to an external driving field, that can describe the process of phase separation of two stable phases.
- $\Gamma(x-x')$ is a distribution that can have different expressions, implying different conservation laws:

- **dynamics with no local conservation of the order parameter (NCOP)** is obtained when

$$\Gamma(x-x') = \Gamma\delta(x-x') \rightarrow \frac{\partial\phi(x,t)}{\partial t} = -\Gamma \frac{\delta\mathcal{H}[\phi]}{\delta\phi(x',t)} + \eta(x,t) \quad (2.3)$$

this equation is also known as **MODEL A** in the Hohenberg-Halperin [25] classification. A dynamics of this type describes for example alloys that undergo an order-disorder transition on cooling through T_c , rather than phase separating. The microscopic counterpart of this model is the **Glauber dynamics** [26].

- **dynamics with local conservation of the order parameter (COP)** is obtained

$$\Gamma(x-x') = -\Gamma\nabla^2\delta(x-x') \rightarrow \frac{\partial\phi(x,t)}{\partial t} = \Gamma\nabla^2 \frac{\delta\mathcal{H}[\phi]}{\delta\phi(x',t)} + \eta(x,t) \quad (2.4)$$

this equation is also known as **MODEL B** in the Hohenberg-Halperin classification [25]. A dynamics of this type describes for example a binary alloy, where it's clear physically that atoms of the two different species can exchange only locally (not over large distances), leading to diffusive transport of the order parameter. The microscopic counterpart of such model is the **Kawasaki dynamics** [27].

After performing a quench, the process described by these equations is characterized by different temporal stages. In an **early stage** (as a linear stability analysis can prove) initial conditions and thermal fluctuations play a role. If, after the quench, the system is in an **unstable state**, i.e. it is described by a point under the spinodal line (Fig. 2.1), a second order transition occurs, where the mixed phase becomes globally unstable (Fig 2.4a) and large-scale critical fluctuations

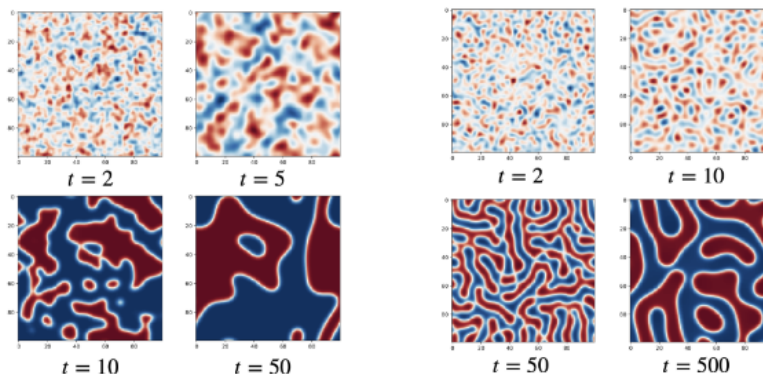


Figure 2.3: Temporal snapshots of phase separation process in case of non-conserved(left) and conserved (right) order parameter. Ref [28]

emerge with essentially no nucleation barrier. Fluctuating domains settle below the critical point into some characteristic morphology with a typical wavelength (Fig 2.4b) that depends on the conservation laws and may coarsen with time. If the system is in a **metastable** state after the quench, i.e. phase separation begins between the binodal and the spinodal (Fig. 2.1), then a first order transition occurs (Fig 2.4c) and the system needs a large thermal fluctuation to overcome the free energy barrier. This happens through the mechanism of nucleation and growth of a droplet: it is possible to identify a critical radius, function of surface tension and gas supersaturation, beyond which a droplet will have more convenience to grow. Depending on whether the system is in a state of large supersaturation/fast particle diffusion or low supersaturation/diffusion limited growth, growth laws show a different dependence on time.

On the contrary, in a **late stage**, the system has developed well defined interfaces, characterized by surface tension. Surface tension drives the dynamics of phase-separated domains, causing the appearance of **universal scaling laws** that depend only on the quench being critical or subcritical and on conservation laws. It is now well established that a scale-invariant **coarsening** domain mosaic emerges from the solutions to the equations at late times [29]. This morphology is (statistically) independent of time when all lengths are rescaled by a typical domain size $L(t)$ that grows algebraically with time. and is usually written as $L(t) \sim t^z$ with z the dynamical exponent whose value is

$$z = \begin{cases} \frac{1}{2} & \text{NCOP (model A)} \\ \frac{1}{3} & \text{COP (model B)} \end{cases}$$

These scaling laws are important in that they imply different coarsening behaviours of the system depending on the conservation laws. This is because the influence

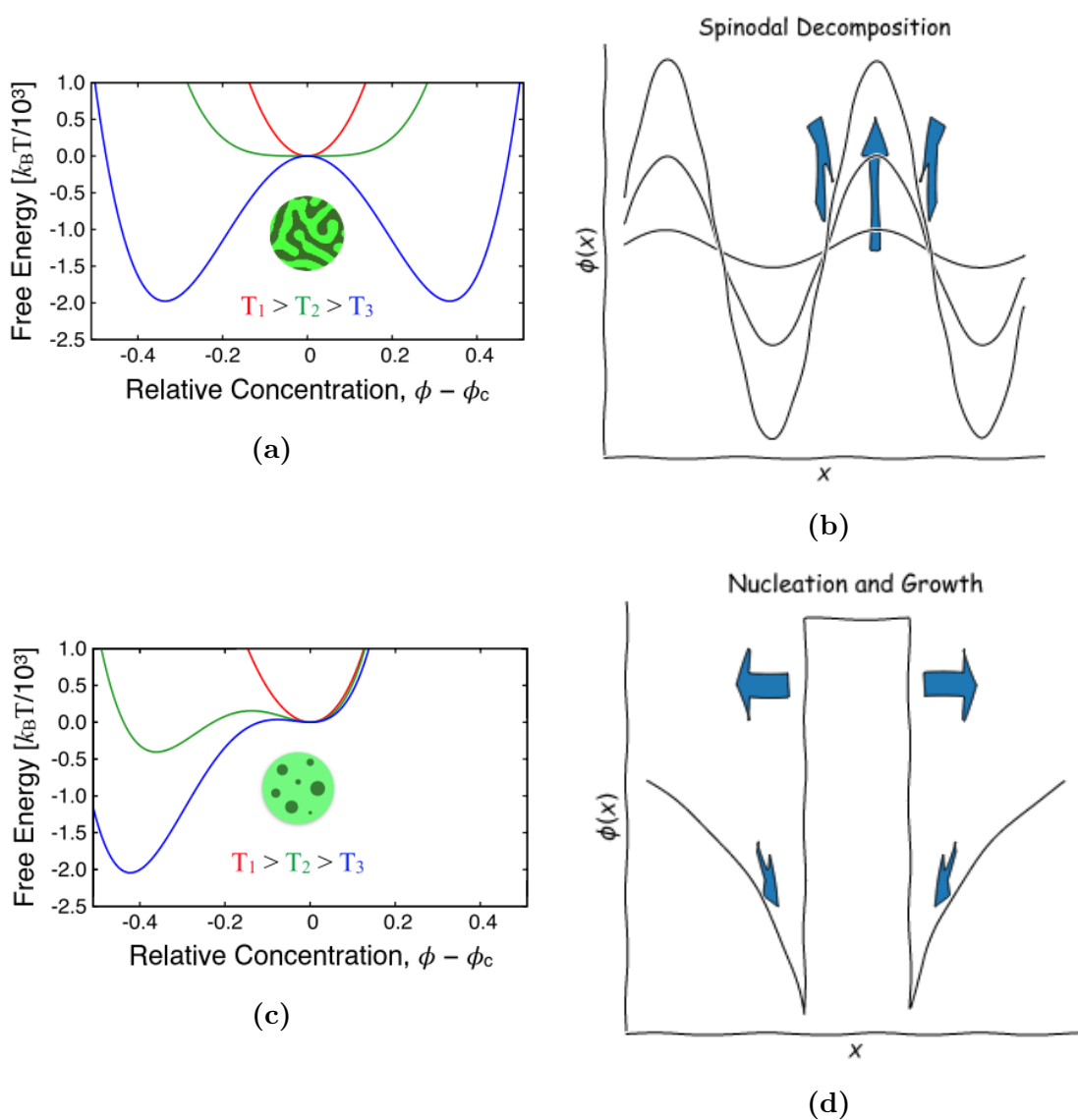


Figure 2.4: (a): Change in the free energy profile when crossing the spinodal line determines the presence of a second order phase transition (from [24]). (b) Mechanism of uphill diffusion occurring during spinodal decomposition drives the system to the development of a characteristic wavelength (from [28]). (c) Change in the free energy profile when crossing the binodal line determines the presence of a first order phase transition. (d) Nucleation and growth mechanism in the metastable region (from [28])

of a conservation law severely limits the way in which an interface between two domains can move.

2.3 Coarsening and competition between domains

A relevant case in cell biology and for this thesis is that of a dilute population of droplets immersed in a majority phase which, at a late stage, coarsen and coalesce, competing for growth. This non trivial dynamics is named *Ostwald Ripening* and results have been obtained for both conserved and non-locally conserved order parameter dynamics. Such results are interesting for the study of domain dynamics on a cell membrane, due to the existence of i) molecular species that mainly diffuse laterally along the membrane (their concentration field is thus locally conserved), ii) molecular species that can shuttle between membrane and cytosol, (thus they introduce a concentration field that is locally non conserved). Emerging scaling laws show that non-locally-conserved dynamics is characterized by a faster coarsening, suggesting that the shuttling mechanism observed in cells may have come as an evolutionary advantage.

2.3.1 Conserved dynamics

To understand the coarsening of a dilute population of droplets it is useful to first look at the scenario of a **single droplet in its supersaturated vapor** (the average concentration \bar{c} of the minority phase in the entire system is larger than the supersaturation value c_∞), in the assumption that the growth of the droplet is governed by diffusion of molecules to it. The following steps are mainly referred to [29]. Under a quasi-static assumption the vapor concentration for the surrounding gas is the solution of a Laplace equation with Dirichlet boundary condition. Thus, concentration profile in 3D follows the expression (see also Fig. 2.5):

$$c(r) = \bar{c} - [\bar{c} - c(R)] \frac{R}{r} \quad (2.5)$$

with $c(R)$ being determined by the Gibbs-Thomson relation (for a possible derivation see for example [30] - Appendix N):

$$c(R) = c_\infty \left(1 + \frac{\nu}{R} \right) \quad (2.6)$$

ν is the capillary length, that is related to the surface tension and the temperature.

Considering that the volume of a droplet changes with time following

$$\frac{dV}{dt} = 4\pi R^2 \frac{dR}{dt} = 4\pi R^2 D \left. \frac{\partial c}{\partial r} \right|_{r=R} \quad (2.7)$$

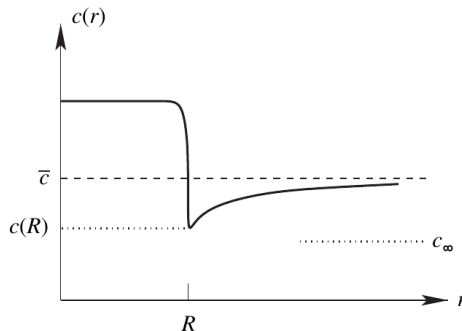


Figure 2.5: Schematic (not to scale) dependence of the minority-phase concentration as a function of the radial coordinate. Figure from [29].

the previous equations allow to calculate the evolution of R , giving

$$\frac{dR}{dt} = \frac{D}{R} \left(\Delta - c_\infty \frac{\nu}{R} \right) = \frac{\alpha}{R^2} \left(\frac{R}{R_c} - 1 \right) \quad (2.8)$$

where $\Delta = \bar{c} - c_\infty$ is the degree of supersaturation and it is possible to identify a critical radius $R_c = \frac{c_\infty \nu}{R}$ such that

$$\begin{cases} R \gg R_c \implies R(t) \text{ grows as } t^{1/2} \\ R < R_c \implies R(t) \text{ shrinks as } t^{1/3} \end{cases}$$

Subcritical droplet shrinkage with $t^{1/3}$ dependence is the building block of $t^{1/3}$ coarsening characterizing conserved order-parameter dynamics, that can be found in the case of **many competing domains**. A system like this was studied by **Lifshitz-Slyzov and Wagner** [31] under the assumptions of a slightly supersaturated background (so that there is competition among domains) and of a dilute population of droplets (so that droplets are non interacting and the concentration field around each droplet is the same as for an isolated droplet). In a scenario like this, where droplets have different sizes, the value of R_c must be determined self consistently. The result of this dynamics is that as time passes, fewer droplets will be found in the system, but will have a larger size, since largest droplets grow up as a result of the swallowing up of the smaller ones. The governing equation are:

- continuity equation for the concentration of droplets of radius R (the flux is defined as $J = f(R, t) \frac{dR}{dt}$):

$$\frac{\partial f}{\partial t} + \frac{\partial J}{\partial R} = 0 \quad (2.9)$$

- Equation 2.8 for the evolution of the radius of a single domain
- conservation of the total mass of the minority phase

$$\bar{c} - c_\infty + \frac{4\pi}{3} \int_0^\infty R^3 f(R, t) dR = \text{const} \quad (2.10)$$

In the minority limit the volume fraction of the minority phase that exists as freely diffusing monomers is vanishingly small. As a consequence the conservation law reduces to the condition that the total volume of the droplets is fixed, ie

$$\int_0^\infty R^3 f(R, t) dR = \text{const} \quad (2.11)$$

A solution for the domain size distribution $f(R, t)$ can be found under the scaling assumption:

$$f(R, t) = \frac{1}{R_c^4} \phi(x) \quad x = \frac{R}{R_c}$$

Such a choice is supported by the fact that it allows to rewrite 2.11 as $\int x^3 \phi(x) dx = \text{const}$ that is manifestly time independent. Substituting this Ansatz in the continuity equation 2.9 it is possible to find the time behaviour for the critical radius

$$R_c \sim t^{\frac{1}{3}}$$

and an expression for ϕ (plotted in Fig.2.6):

$$\phi(x) = \begin{cases} Cx^2(3+x)^{-7/3}(3-2x)^{-11/3}e^{-\frac{3}{3-2x}} & x < \frac{3}{2} \\ 0 & x \geq \frac{3}{2} \end{cases}$$

with the amplitude C fixed by the conservation law 2.11.

This last result leads to the average size of domains scaling in time as $\langle R(t) \rangle \sim t^{1/3}$. Such slower-than-diffusive behaviour also justifies the quasi-static approximation that was used to determine the concentration outside a droplet. It's important to point out that this derivation holds only for $d > 2$, however the same qualitative behaviour is found for arbitrary dimension: for $d = 2$, in particular, there are rather relevant logarithmic corrections whose final effect is not universal and results in a slowing down of the dynamics.

2.3.2 Non conserved dynamics

Exploiting scaling assumptions it is also possible to derive the scaling behaviour of domain size distribution in the case of a **non conserved order parameter**,

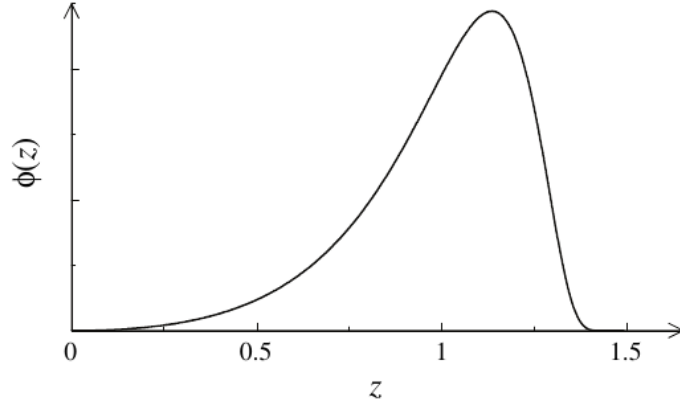


Figure 2.6: Plot of ϕ . From [29]

as done in [32]. By Allen-Cahn equation (see for example [30]-Appendix O) the local velocity of a domain wall in any dimension is proportional to its curvature, meaning that in two dimensions the area of the domain shrinks with constant rate (let us say $\frac{dA}{dt} = -\lambda$). As a consequence of this, the domain size distribution satisfies the continuity equation

$$\frac{\partial}{\partial t}f(A, t) + \frac{\partial}{\partial A}(-\lambda f(A, t)) = 0$$

giving $f(A, t) = \frac{C}{(A+\lambda t)^2}$ that comes with the scaling $R(t) \sim t^{\frac{1}{2}}$.

Results have also been found for the case of a **non locally conserved order parameter, with global conservation, for $d = 2$** , in order to address the problem of domain coalescence on cell membrane [8],[33] (see Fig.2.7a). In this case the system is dominated by the equations (Δ is the degree of metastability, σ the linear surface tension, and γ is a damping factor):

- time evolution of the distribution function $f(R, t)$ for the domain radius R :

$$\gamma \frac{\partial f}{\partial t} + \frac{\partial}{\partial R}[(\Delta - \frac{\sigma}{R})f] = 0 \quad (2.12)$$

- degree of metastability $\Delta(t)$ tends to zero at the equilibrium, as the total patch area tends to its limit value A_{TOT} :

$$\Delta \propto A_{TOT} - \int dR \pi R^2 f(t, R) \quad (2.13)$$

Asymptotically these equations lead to the self similar solution

$$\Delta(t) = (2\sigma\gamma/t)^{\frac{1}{2}} \quad f \propto t^{-\frac{3}{2}} g(\sqrt{\gamma}R/\sqrt{2\sigma t})$$

implying $\langle R \rangle = \sigma/\Delta = R_c$ and therefore $\langle a \rangle \propto \Delta^{-1} \propto \sqrt{t}$. The evolution of the self similar domain size distribution is plotted in figures 2.7a, 2.7b. This result is interesting because it is reminiscent of the Landau-Slyzov-Wagner theory of coarsening, showing a peak in the distribution of domains due to global conservation, but the dynamics is faster due to the scaling $R(t) \sim t^{\frac{1}{2}}$.

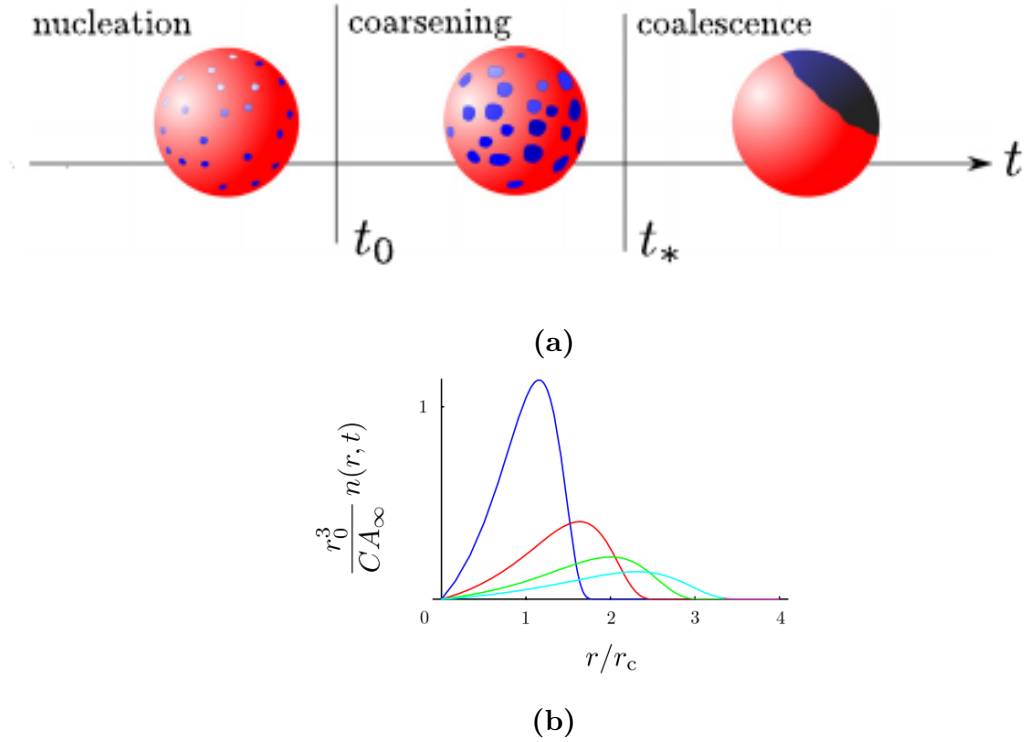


Figure 2.7: (a) Domain coarsening and coalescence during cell polarization. (b) Time evolution of the self similar domain size distribution ($t/t_0 = 1,2,3,4$). Figures from [33].

Chapter 3

Phase separation in molecular sorting: one-component model

*“Will I see you give more than I can take?
Will I only harvest some?”
Neil Young, Harvest*

As claimed recently [22, 23], the process of molecular sorting may emerge from the combination of two fundamental physical processes: a) a phase separation of specific molecules into localized sorting domains and b) domain induced membrane bending, leading to the formation of vesicles enriched in the biochemical factors of the engulfed domains. This means that the process can be modelled, in abstract and phenomenological terms, as a scenario in which **proteins arrive on a membrane region, diffuse and, due to an attractive interaction, aggregate into localized enriched domains which are removed from the membrane after reaching a characteristic size $R_E \gg R_c$** : this mimics vesicle extraction at a coarse grained level, without introducing explicitly membrane dynamics and scission process. Direct coalescence of domains is not included in the model because diffusivity of clusters in the membrane is much smaller than that of single molecules (see [22], Supplementary Material), Such a model can be considered a variant of the Island Growth model [29] for aggregation with input, with the difference that in the present case over-threshold domains are removed and the aggregation is not irreversible: according to classical nucleation theory, a critical size A_c is required for a domain to continue to grow and avoid decay. At the stationary state the growing domains coexist with a continuously repleted two-dimensional gas: if the supersaturation is low the domains compete for growth and the scenario is

then reminiscent of 2D diffusion-limited-aggregation and Lifshitz-Slyzov-Wagner coarsening (but in 2D). Two important differences from the LSW coarsening are, however, that 1) the solution is constantly repleted 2) extraction of over-threshold domains prevents complete coalescence to be reached. In such a framework it is natural to ask when sorting is most efficient and how is the size of domains statistically distributed in such optimal condition. The **efficiency of the sorting process** can be measured in terms of the average residence time \bar{T} of a molecule on the membrane system, that is proportional to the density of molecules on the membrane (see [34]).

Useful scaling laws governing the system can be derived by exploiting the parallelism with Ostwald-ripening and thus following a similar approach to the ones introduced in Sec.2.3. In a slight supersaturation scenario, the system can be thought as divided in many attracting basins and the "vapor" density $n(r)$ surrounding a domain can be found, with a quasi-static assumption, by solving a Laplace equation in two dimensions with Dirichlet boundary conditions:

$$n(r) = n_0 + \frac{\ln(r/R)}{\ln(L/R)} \Delta n \quad (3.1)$$

where \bar{n} is average molecule density in the gas, that can be considered constant by continuous repletion of molecules, n_0 the molecule density in proximity to the domain boundaries and $\Delta n = \bar{n} - n_0$. R is the radius of the domain (approximating a domain as circular) and L the typical inter-domain distance. The evolution of the system is then governed by the following equations:

- **Dynamic equation for domain growth** (with $A_0 =$ area occupied by a molecule in the domain):

$$\dot{R} = A_0 D \Delta n / [R \ln(L/R)] \quad (3.2)$$

This expression can be obtained from the flux of molecules from the gas

$$\Phi_R = 2\pi R D \partial_r n(r) \Big|_{r=R} = \frac{2\pi D \Delta n}{\ln(L/R)} \quad (3.3)$$

that is related to radius dynamics by $\dot{R} = \frac{1}{2\pi R} \Phi_R A_0$

- **Smulochowski equation** describing the statistics of supercritical domains $N(t, R)$ (defined such that $N(t, R)dR$ is the number of domains per unit area with size between R and $R + dR$):

$$\frac{\partial N}{\partial t} + \frac{\partial}{\partial R}(\dot{R}N) = -\gamma(R)N \quad (3.4)$$

where $\gamma(R)$ is the extraction rate for domains of size R and is assumed to be negligible if $R < R_E$, while it is strong for $R > R_E$. This expression is analogous to Eq.2.9, with the difference that the l.h.s. term is not zero and models domain extraction.

Together, Eq.3.2 and 3.4 bring to the stationary solution

$$N_{st}(R) = \frac{JR \ln(L/R)}{D\Delta R} \exp - \int_0^R dr \frac{r \ln(L/r) \gamma(r)}{A_0 D \Delta n} \quad (3.5)$$

where the factor J can be determined imposing that at stationarity the average flux to the domains equate the incoming flux ϕ per unit area

$$\int dR \Phi_R N_{st}(R) \sim \phi \quad (3.6)$$

giving

$$J \sim \frac{\phi}{R_E^2} \quad (3.7)$$

The distribution is plotted in Fig. 3.1 (red line).

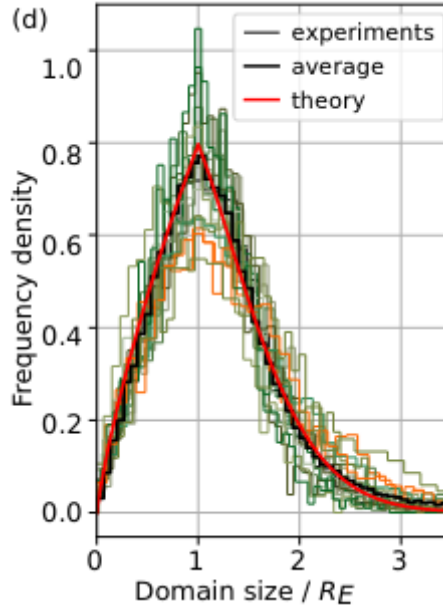


Figure 3.1: Frequency densities of domain sizes during the sorting process, accordance between the phenomenological theory (Eq.3.5), experiments and simulations, Ref. [22]

This result is useful to evaluate the efficiency of the sorting process by allowing to estimate the average residence time \bar{T} of a molecule on a membrane system,

which can be written as the sum of the average time \bar{T}_f required to reach a domain by free diffusion and be absorbed and the average time \bar{T}_d spent inside the domain until the extraction event. Notice that an absorbing domain is implicitly assumed: this simplification assumes a small critical size and thus neglects the time spent in under-critical domains. The two terms can be estimated as follows:

- \bar{T}_f should be inversely proportional to the expected number of domains and to diffusivity, giving

$$\bar{T}_f \sim 1/(DN_d) \sim \Delta n/\phi \quad (3.8)$$

where $N_d = \int dR N_{st}(R) \sim \phi/(D\Delta n)$

- \bar{T}_d can be approximated to the time required to a flow of molecules to fill an area $\sim R_E^2$

$$\bar{T}_d \sim R_E^2/(A_0\Phi_R) \sim R_E^2/(D_0\Delta n) \quad (3.9)$$

A scaling form for \bar{n} can be found considering the rate of formation of domains, that can be estimated as

$$dN_d/dt = CD\bar{n}^2 \quad (3.10)$$

where C is a dimensionless quantity characterizing the efficiency of absorption of single molecules by a germ of a domain. At stationarity this rate equates the rate at which a domain is extracted from the system

$$dN_d/dt = N_d/\bar{T}_d \quad (3.11)$$

and we can thus find a scaling form for \bar{n}

$$\bar{n} \sim \left(\frac{\phi A_0}{CDR_E^2} \right)^{1/2} \quad (3.12)$$

Under the assumption of a strong depletion around a domain it is possible to approximate $\Delta n \sim \bar{n}$ and then substitute this scaling form in the expression for $\bar{T} = \bar{T}_f + \bar{T}_d$, obtaining that it has a minimum for $C \sim A_0^2/R_E^2 \ll 1$

Such result has been confirmed numerically through a lattice-gas microscopic model, where the system evolves according to a Markov process that comprises the following three elementary mechanisms:

1. molecules from an infinite reservoir arrive and are inserted on empty sites with rate k_I
2. molecules can perform diffusive jumps to an empty neighboring site with rate $k_D/g^{N_{nn}}$, where N_{nn} is the number of molecules neighboring and where $g > 1$
3. molecules are extracted from the system by the simultaneous removal of all connected molecule clusters, if any, that contain a completely filled square of linear size l , with $l^2 \sim R_E/A_0$

Efficiency of the process can be evaluated by measuring the density ρ , that is proportional to \bar{T} . As can be seen in Fig. 3.2a results confirmed the estimates, in that C increases monotonically and non-linearly with the aggregation coefficient g . Experimentally measured densities are reached in the physical model near the density minima (Fig. 3.2b), supporting the idea that evolution may have led proteins to tune their activity around optimality.

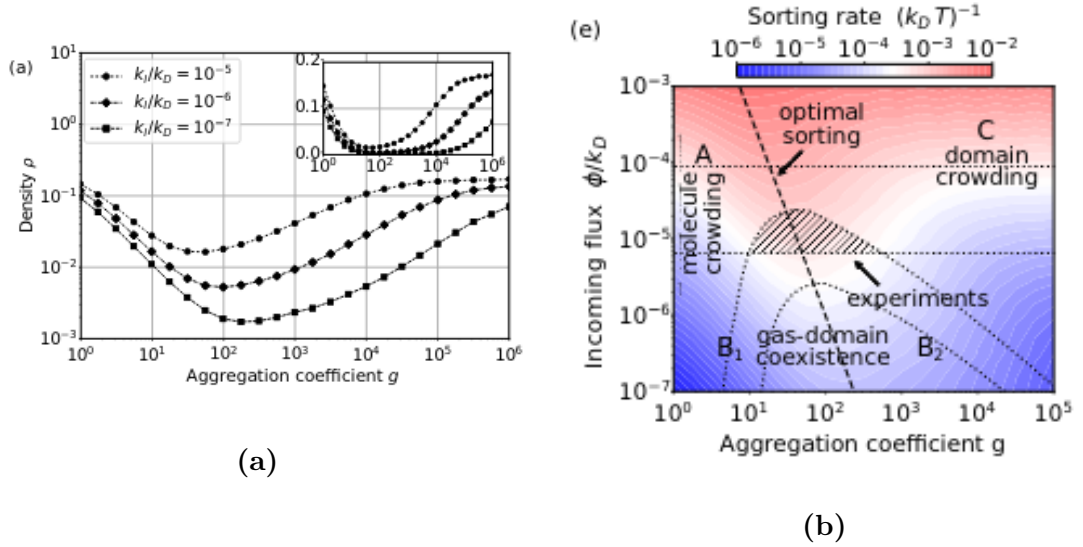


Figure 3.2: (a): density obtained at the stationary state (from numerical simulations) as a function of the aggregation coefficient g , for different incoming fluxes. (b): nondimensionalized sorting rate as a function of the aggregation coefficient g and of the nondimensionalized incoming flux. Values obtained from experiments on living cells are compatible with the idea that cells operate in an optimal regime. From [22]

Chapter 4

Phase separation in molecular sorting: introducing a two-component model

*“Hey, Hey, What Can I Do
Led Zeppelin*

Despite being minimal, the model discussed in [22] and presented in the previous chapter proved capable to capture a crucial feature of the sorting process, that is the existence of an optimal region in which the process takes place. Having a minimal model capable to do this is an important point, since it means that the feature investigated is robust (i.e. it does not rely on details of the system). Encouraged by these results, this work aims to add new ingredients to the model, while keeping it minimal. So far, only one type of molecule has been considered, which, once inserted in the membrane, can only diffuse until it is extracted together with a over-threshold domain; however, as pointed out in Ch.1, coat formation involves the interaction of:

1. **cargo molecules**, that are an input to the system and, once present on the membrane, can mainly *diffuse* until they are extracted.
2. a *finite* pool of cytosolic **endocytic proteins** of different types that can *shuttle* between membrane and cytosol (i.e: they evaporate from any part of the membrane, then they diffuse rapidly in the cytosol and are successively captured again in another part of the membrane) and are *recycled* after an

extraction event. This is the case, for example, of adaptor molecules and clathrins. In the following these proteins will be referred, in general, as “auxiliary molecules”

Imagining to focus on a small region of the membrane for relatively short time scales (shorter than the typical time scale of domain growth and extraction and of cargo insertion) we would see that the concentration field of the cargo is locally conserved on the membrane (“model B” following the classification in [25]). On the contrary, the fast redistribution mechanism followed by the auxiliaries implies that their concentration field is approximately globally - but not locally - conserved on the membrane (“model A” following the classification in [25], but with global conservation).

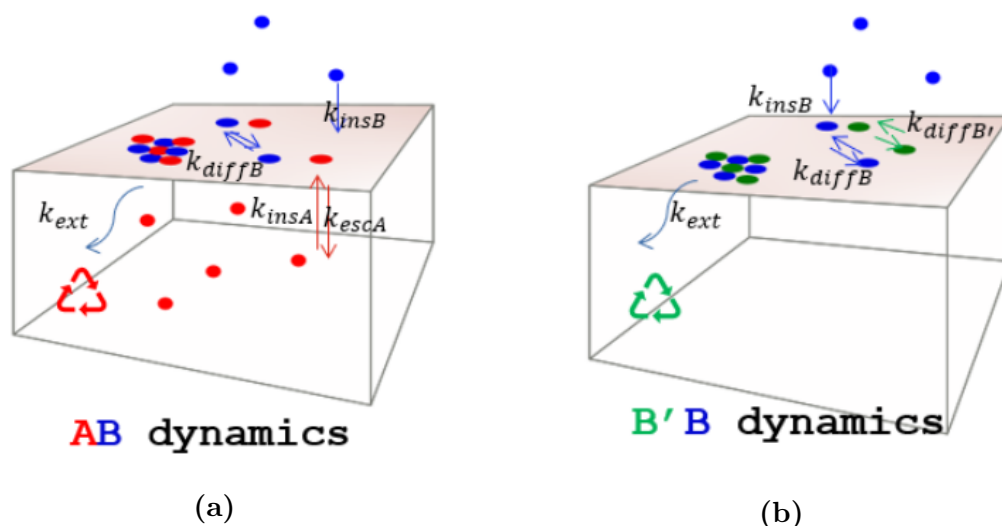


Figure 4.1: (a):AB model (b) B'B model

With these observations in mind, in the following I am going to propose a “**AB model**” in order to answer the following questions:

- Q1** What are the crucial features of such a coupled dynamics?
- Q2** According to classical theories of phase separation (see Ch. 2) systems that follow a A dynamics show a faster coarsening. At the same time in [22] it was found that optimality takes places in scenarios where the number of sorting domains is minimized (few overcritical domains) suggesting that faster coarsening might facilitate sorting. So, does the interaction of cargoes with molecules that follow a faster, non-locally-conserved dynamics, make the process more efficient?

4.1 AB model

The **membrane** system is modelled as a **2D lattice-gas** with periodic boundary conditions, which is coupled to an **unstructured cytosol**. As discussed in Ch.1 there are tens of protein types involved in the process of protein sorting, however here I follow a coarse-grained approach and consider the interactions of just two types of “particles”, “B particles” and “A particles”, that model respectively cargo and auxiliary molecules:

B particles allowed to perform two moves:

Insertion on the membrane from a *infinite* reservoir (this is because they mimic cargoes, that are an *input* to the system) such that an empty site of the membrane will be occupied by a B particle with a rate

Diffusion to a neighboring empty site with rate $\frac{k_{\text{diffB}}}{g^{n_A}}$, where n_A counts the number of first-neighbouring A particles. k_{diffB} is the diffusion rate for a free molecule and g the adimensional aggregation constant.

When an over-threshold domain is extracted the B particles involved are just removed from the system.

A particles allowed to perform:

Insertion on the membrane from a finite reservoir (at each time step $N_{\text{Atot}} = N_{\text{Acyt}} + N_{\text{Amem}}$) such that the rate at which an empty site can be occupied by an A molecule is $k_{\text{insA}} N_{\text{Acyt}}$

Detachment with the position dependent rate $\frac{k_{\text{detA}}}{g^{n_B}}$, where n_B counts the number of first-neighbouring B particles and k_{detA} is the detachment rate for a free particle

When an over-threshold domain is extracted the A particles involved are re-immitted in the cytosol.

A connected component of at least N_E elements is extracted with rate k_{ext} . In this work it is assumed that A-A and B-B interactions are of excluded volume type, while a contact attractive potential is assumed for A-B interactions, modelling the cargo-auxiliary molecule affinity presented in Ch.1. A more realistic model could assume an attractive interaction also between homologous particles, indeed as I claimed in Ch.1, there is a cooperation between auxiliary molecules (see Fig. 1.8): in other words in a more general case we would have an aggregation matrix

$$G = \begin{bmatrix} g_{AA} & g_{AB} \\ g_{AB} & g_{BB} \end{bmatrix}$$

that is now simplified to

$$G = \begin{bmatrix} 1 & g \\ g & 1 \end{bmatrix}$$

. This assumption is needed to reduce the number of parameters and at the same time is consistent with the fact that domains need both cargo and auxiliary molecules in order to be stable (see Ch.1).

4.2 B'B model

The AB model defined previously has three crucial features:

1. finite and conserved pool of auxiliary molecules
2. auxiliary molecules perform a A dynamics
3. attractive interaction only for A-B pairs

So, in order to assess what contribution is given by the shuttling property of the auxiliary molecules, I introduce a “B'B” model that shares features 1) and 3) with model AB but it replaces A particles with **B' particles**, that can jump to empty neighbouring sites with rate $\frac{k_{\text{diffB}'}}{g^{n_B}}$ - and thus follow a B dynamics - and are recycled after an extraction event (they are re-inserted randomly on the membrane). .

4.3 Parameter dependence

As in [22], we are interested at evaluating the efficiency of the process by calculating the density of molecules achieved by the system at stationarity, that is a relevant situation that happens often in biological and non biological systems. In the microscopic model we can define $\rho = \frac{\text{Number of filled sites}}{\text{Total number of sites}}$ such that $[\rho] = 1$ (i.e. ρ is nondimensional). In general, at stationarity this quantity for the AB model is given by

$$\rho_{\text{AB}} = \rho_{\text{AB}}\left(g, \frac{N_{\text{aux}}}{N_{\text{sites}}}, N_{\text{ext}}, k_{\text{ext}}, k_{\text{insA}}, k_{\text{detA}}, k_{\text{insB}}, k_{\text{diffB}}\right) \quad (4.1)$$

A choice for the extraction threshold can be $N_{\text{ext}} = 100$, that is a reasonable value since the lateral surface occupied by a protein is typically $A_0 \sim (10\text{nm})^2$ [15] and the size of mature endocytic vesicles is $A_E \sim (100\text{nm})^2$ [22]. We are thus left with

$$\rho_{\text{AB}} \Big|_{N_{\text{ext}}=100} = \rho_{\text{AB}} \Big|_{N_{\text{ext}}=100} \left(g, \frac{N_{\text{aux}}}{N_{\text{sites}}}, k_{\text{ext}}, k_{\text{insA}}, k_{\text{detA}}, k_{\text{insB}}, k_{\text{diffB}}\right) \quad (4.2)$$

Since $[\rho_{\text{AB}}] = \left[\frac{N_{\text{aux}}}{N_{\text{sites}}}\right] = 1$ and $[k_{\text{detA}}] = [k_{\text{diffB}}] = [k_{\text{insB}}] = [k_{\text{ext}}] = \frac{1}{[\text{time}]}$ we can write, in a similar fashion of [22]

$$\rho_{\text{AB}} \Big|_{N_{\text{ext}}=100} = \rho_{\text{AB}} \Big|_{N_{\text{ext}}=100} \left(g, \frac{N_{\text{aux}}}{N_{\text{sites}}}, \frac{k_{\text{ext}}}{k_{\text{diffB}}}, \frac{k_{\text{insA}}}{k_{\text{diffB}}}, \frac{k_{\text{detA}}}{k_{\text{diffB}}}, \frac{k_{\text{insB}}}{k_{\text{diffB}}}\right) \quad (4.3)$$

The number of parameters can be reduced assuming that

- $k_{\text{ext}} \rightarrow \infty$ (i.e. the precise value of the extraction rate is irrelevant as long as the extraction dynamics is much faster than the characteristic timescale of domain growth, so that similar scenarios are always observed for large but finite values of k_{ext}).
- we take the limit $k_{\text{insA}} \rightarrow \infty$: this is compatible with the assumption of a fast diffusion of auxiliaries in the cytosol

and obtaining (the $\hat{\cdot}$ indicates the assumptions done)

$$\hat{\rho}_{AB} = \hat{\rho}_{AB}(g, \frac{N_{\text{aux}}}{N_{\text{sites}}}, \frac{k_{\text{detA}}}{k_{\text{diffB}}}, \frac{k_{\text{insB}}}{k_{\text{diffB}}}) \quad (4.4)$$

Similarly, for the B'B model we have

$$\rho_{B'B} = \rho_{B'B}(g, \frac{N_{\text{aux}}}{N_{\text{sites}}}, N_{\text{ext}}, k_{\text{ext}}, k_{\text{diffB}'}, k_{\text{insB}}, k_{\text{diffB}}) \quad (4.5)$$

that, following similar steps, becomes

$$\rho_{B'B} \Big|_{N_{\text{ext}}=100} = \rho_{B'B} \Big|_{N_{\text{ext}}=100} (g, \frac{N_{\text{aux}}}{N_{\text{sites}}}, \frac{k_{\text{diffB}'}}{k_{\text{diffB}}}, \frac{k_{\text{insB}}}{k_{\text{diffB}}}) \quad (4.6)$$

In a first approximation lateral diffusivity of different species along the membrane should not vary much in terms of order of magnitude, so we can assume $\frac{k_{\text{diffB}'}}{k_{\text{diffB}}} = 1$, getting

$$\hat{\rho}_{B'B} = \hat{\rho}_{B'B}(g, \frac{N_{\text{aux}}}{N_{\text{sites}}}, \frac{k_{\text{insB}}}{k_{\text{diffB}}}) \quad (4.7)$$

To sum up we have

$$\hat{\rho}_{AB} = \hat{\rho}_{AB}(g, \frac{N_{\text{aux}}}{N_{\text{sites}}}, \frac{k_{\text{detA}}}{k_{\text{diffB}}}, \frac{k_{\text{insB}}}{k_{\text{diffB}}})$$

$$\hat{\rho}_{B'B} = \hat{\rho}_{B'B}(g, \frac{N_{\text{aux}}}{N_{\text{sites}}}, \frac{k_{\text{insB}}}{k_{\text{diffB}}})$$

The system was studied by running simulations based on the algorithm described in Ch.5, obtaining phase diagrams as a function of g and $\frac{N_{\text{aux}}}{N_{\text{sites}}}$. Simulations were performed on a 200x200 square lattice with periodic boundary conditions setting $\frac{k_{\text{insB}}}{k_{\text{diffB}}} = 10^{-6}$. To make a comparison as direct as possible between model AB and model B'B I first set $k_{\text{detA}} = k_{\text{diffB}} = k_{\text{diffB}'}$: in this case we are ultimately comparing a model where the auxiliary molecules perform a random walk on a square grid (the B'B model) with the case where they still perform a random walk, but the steps, even if with the same propensity, can have arbitrary length and direction. For the AB model I then also investigated the case where $\frac{k_{\text{detA}}}{k_{\text{diffB}}} = 10^2$ in order to study the role of a faster redistribution of the auxiliaries (the larger k_{detA} the lower is the affinity of the auxiliaries for the membrane in absence of cargo).

Chapter 5

Model and Algorithm

*"This means war
With your creator"
Muse, Algorithm*

5.1 Model formalization

The kinetic of distillation in the model AB can be described as a **continuous time Markov process** specified by the infinitesimal generator L . Given, $Col = \{A, B\}$, $\eta \in Col^N$ the configuration of the system, $f(\eta)$ a function of the state of the system (such as density of molecules), L is defined by the relation

$$\partial_t \mathbb{E}(f(\eta)) = \mathbb{E}(Lf(\eta)) \quad (5.1)$$

where $\mathbb{E}(f(\eta)) = \sum_{\eta} P(\eta) f(\eta)$. and L is given by the sum

$$L = L_{\text{insB}} + L_{\text{diffB}} + L_{\text{insA}} + L_{\text{detA}} + L_{\text{ext}} \quad (5.2)$$

where the various contributions are defined in the following way:

L_{insB} operator for the insertion of a B particle:

$$L_{\text{insB}} f(\eta) = k_{\text{insB}} \sum_{i:\eta_i=0} [f(\eta^{iB}) - f(\eta)] \quad (5.3)$$

where the configuration η^{iB} differs from η only for the insertion of a B particle on site i .

L_{insA} operator for the insertion of a A particle:

$$L_{\text{insA}} f(\eta) = N_{\text{cyt}}^A k_{\text{insA}} \sum_{i:\eta_i=0} [f(\eta^{iA}) - f(\eta)] \quad (5.4)$$

L_{diffB} -operator for the diffusion of a B particle:

$$L_{\text{diffB}}f(\eta) = k_{\text{diffB}} \sum_{i:\eta_i=B} \sum_{j \in \mathcal{N}_i, \eta_j=0} g^{-n_A(i)} [f(\eta^{ij}) - f(\eta)] \quad (5.5)$$

where η^{ij} differs from η only for the jump of molecule in site i to site j and $n_A(i)$ is the number of A particles neighbouring site i .

L_{detA} operator for the detachment of a A particle:

$$L_{\text{detA}}f(\eta) = k_{\text{detA}} \sum_{i:\eta_i=A} g^{-n_B(i)} [f(\eta^{-iA}) - f(\eta)] \quad (5.6)$$

where $n_B(i)$ is number of B particles neighbouring site i . η^{-iA} differs from η only for the detachment of a A particle in site i .

L_{ext} operator for the extraction of a connected over-threshold cluster:

$$L_{\text{ext}}f(\eta) = k_{\text{ext}} \sum_{C \in \mathcal{C}} [f(\eta^C) - f(\eta)] \quad (5.7)$$

where \mathcal{C} is the set of connected clusters above threshold and η^C differs from η only for the removal of a cluster C (so we set $\eta_i = 0 \forall i \in C$)

The infinitesimal generator for the B'B model can be written as

$$L = L_{\text{insB}} + L_{\text{diffB}} + L_{\text{diffB}'} + L_{\text{ext}} \quad (5.8)$$

with

$$L_{\text{diffB}'}f(\eta) = k_{\text{diffB}'} \sum_{i:\eta_i=B'} \sum_{j \in \mathcal{N}_i, \eta_j=0} g^{-n_B(i)} [f(\eta^{ij}) - f(\eta)] \quad (5.9)$$

the infinitesimal generator for the diffusion of a B' particle.

5.2 Gillespie algorithm

5.2.1 Basic ideas

To simulate the system a Gillespie (Kinetic Monte Carlo) algorithm [35] was implemented, which is a rejection-less Monte Carlo algorithm commonly used to simulate stochastic processes in continuous time. We first recall here some of the basic ideas behind this algorithm and then focus on our specific implementation. Let's consider n independent events and set $p_i = \Delta t \bar{p}_i$ (\bar{p}_i has thus dimension $1/[time]$) the probability of occurrence of event i in the time interval Δt . If we

suppose to be at instant t , then the probability that next event will happen in an interval $[t + \tau, t + \tau + dt]$ is given by

$$p([t + \tau, t + \tau + dt]) = \left(\sum_{i=1}^N \bar{p}_i \right) e^{-(t+\tau) \sum_{i=1}^N \bar{p}_i} dt \quad (5.10)$$

Memory-less property of Markov processes implies

$$p([\tau, \tau + dt]) = \left(\sum_{i=1}^N \bar{p}_i \right) e^{-\tau \sum_{i=1}^N \bar{p}_i} dt \quad (5.11)$$

and so the waiting time τ follows an exponential distribution

$$\tau \sim \mathcal{E}\left(\sum_{i=1}^N \bar{p}_i\right) \quad (5.12)$$

from which it is possible to sample using the inverse cumulative method, obtaining

$$\tau_{\text{sampled}} = \frac{-\log(1 - u)}{\sum_{i=1}^N \bar{p}_i} \quad (5.13)$$

where $u \sim \mathcal{U}([0,1])$.

Probability that an event i happens, conditioned to the fact that an event happens, is given by

$$p(i \text{ happens} | \text{sth happens}) = \frac{\bar{p}_i}{\sum_{i=1}^N \bar{p}_i} + \mathcal{O}(1) \quad (5.14)$$

According to the inverse cumulative method it is possible to sample from this distribution choosing the event μ such that

$$\frac{\sum_{i=1}^{\mu-1} \bar{p}_i}{\sum_{i=1}^N \bar{p}_i} < r \leq \frac{\sum_{i=1}^{\mu} \bar{p}_i}{\sum_{i=1}^N \bar{p}_i} \quad (5.15)$$

So the structure of the algorithm is given by the repetition of the following steps:

1. initialize configuration
2. draw the waiting time
3. increase clock by τ
4. draw which event will happen
5. update the system, update the possible events that can happen at this current configuration and their relative propensities \bar{p}_i
6. go to 2

5.2.2 Implementation

In the present case things are slightly complicated by the fact that the number of possible events that can potentially happen scales at least with the size of the lattice ($> \mathcal{O}(N_{\text{sites}})$). A strategy to overcome this is to group events that will happen with the same propensity and subsequently draw what specific event among them will happen, conditioned to the fact that one of these events will happen. In our system the propensity of a particle to do a certain move is strictly related to its position. In order to follow this approach it is useful to define the function lc that associates each site to its local configuration

$$lc(i) = (\eta(i), n_{\text{empty}}(i), n_A(i), n_B(i))$$

(where $n_{\text{empty}}(i)$ is the number of neighbouring empty site). With LC_A (LC_B) we denote the space of possible local configurations having respectively a A particle (a B particle) in the middle. It is hence possible to define a vector for the propensities:

$$\vec{\nu} = \begin{bmatrix} \vec{\nu}_{\text{diffB}} \\ \vec{\nu}_{\text{detA}} \\ \vec{\nu}_{\text{ins}} \\ \nu_{\text{ext}} \end{bmatrix}$$

where:

- $\vec{\nu}_{\text{diffB}} \in \mathbb{R}^{|LC_B|}$ is the vector for the propensities of particle B diffusion: given $lc_k = (B, n_{\text{empty}}^k, n_A^k, n_B^k) \in LC_B$ a local configuration, the propensity of having a B particle in that local configuration diffusing is

$$\nu_{\text{diffB}}^{lc_k} = N_{lc_k} k_{\text{diffB}} n_{\text{empty}}^k g^{-n_A^k}$$

with N_{lc_k} the number of particles in that local configuration.

- $\vec{\nu}_{\text{detA}} \in \mathbb{R}^{|LC_A|}$ analogously is the vector such that, given $lc_k = (A, n_{\text{empty}}^k, n_A^k, n_B^k) \in LC_A$,

$$\nu_{\text{detA}}^{lc_k} = N_{lc_k} k_{\text{detA}} g^{-n_B^k}$$

is propensity of having the detachment of a A particle in that local configuration.

- $\vec{\nu}_{\text{ins}} = [\nu_{\text{insA}}, \nu_{\text{insB}}]$ is the vector for the propensities of insertion such that

$$\nu_{\text{insA}} = k_{\text{insA}} N_A^{\text{cyt}} N_{\text{empty}}$$

$$\nu_{\text{insB}} = k_{\text{insB}} N_{\text{empty}}$$

- ν_{ext} tells the propensity of having an extraction event and is given by

$$\nu_{ext} = k_{ext}N_{ot}$$

with N_{ot} being the number of over-threshold domains

So the selected event may be:

- a diffusion of a particle in local configuration lc_k : the algorithm then chooses uniformly at random a site among the ones in that local configuration.
- a detachment of a particle in local configuration lc_l : the algorithm then chooses uniformly at random a site among the ones in that local configuration
- an insertion of a particle of type A or B: the algorithm then chooses uniformly at random an empty site where to insert it
- an extraction of a domain: the algorithm then chooses uniformly at random the connected component whose size is above threshold

Once that the instant for the next event is drawn and the event is selected, the system configuration is updated and the vector of propensities re-calculated. The main steps of the algorithm are illustrated in 5.1

The algorithm for the B'B model is very similar. The vector of rates becomes

$$\vec{\nu} = \begin{bmatrix} \vec{\nu}_{diffB} \\ \vec{\nu}_{diffB'} \\ \vec{\nu}_{insB} \\ \nu_{ext} \end{bmatrix}$$

and the structure of the algorithm is in Fig. 5.2

During the simulation statistics are tracked following the algorithm in Fig.5.3. At the end we are able to compute

- the temporal average in the time window $[t - \Delta t, t]$ as

$$\langle s \rangle(t) = \frac{WS_s(t)}{\Delta t(t)}$$

- the temporal average in the time window $[t_1, t_2]$

$$\langle s \rangle = \frac{\sum_{t=t_0}^{t_2} WS_s(t)}{\sum_{t=t_0}^{t_2} \Delta t(t)}$$

Where $s = \rho, \rho^2, \rho^3, \rho^4$, ρ is the total density of the system and $\rho_{part}^{\vec{}}$ is the vector of the partial densities.



Figure 5.1: Structure of the algorithm used to simulate the AB model

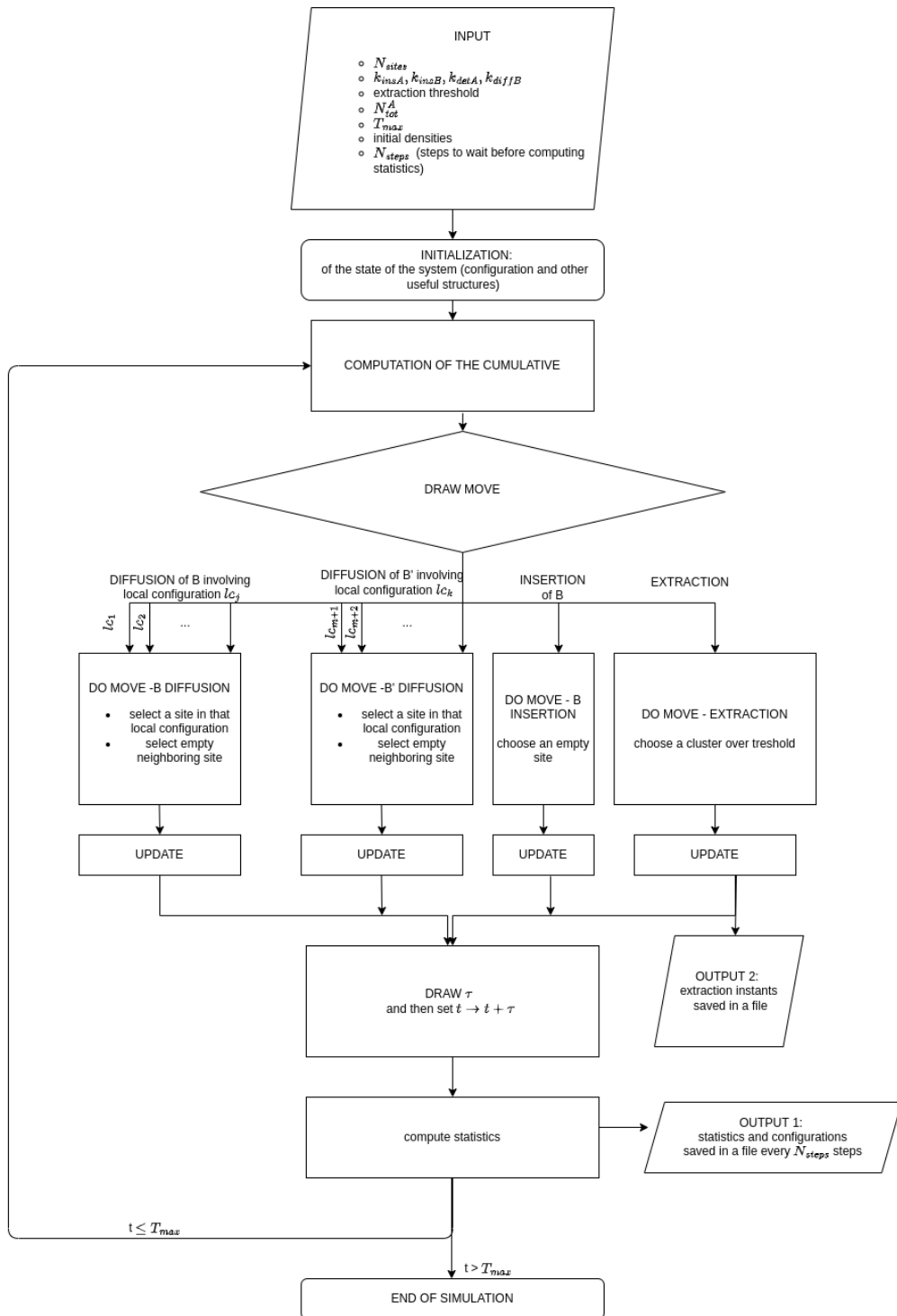


Figure 5.2: Structure of the algorithm used to simulate the B'B model

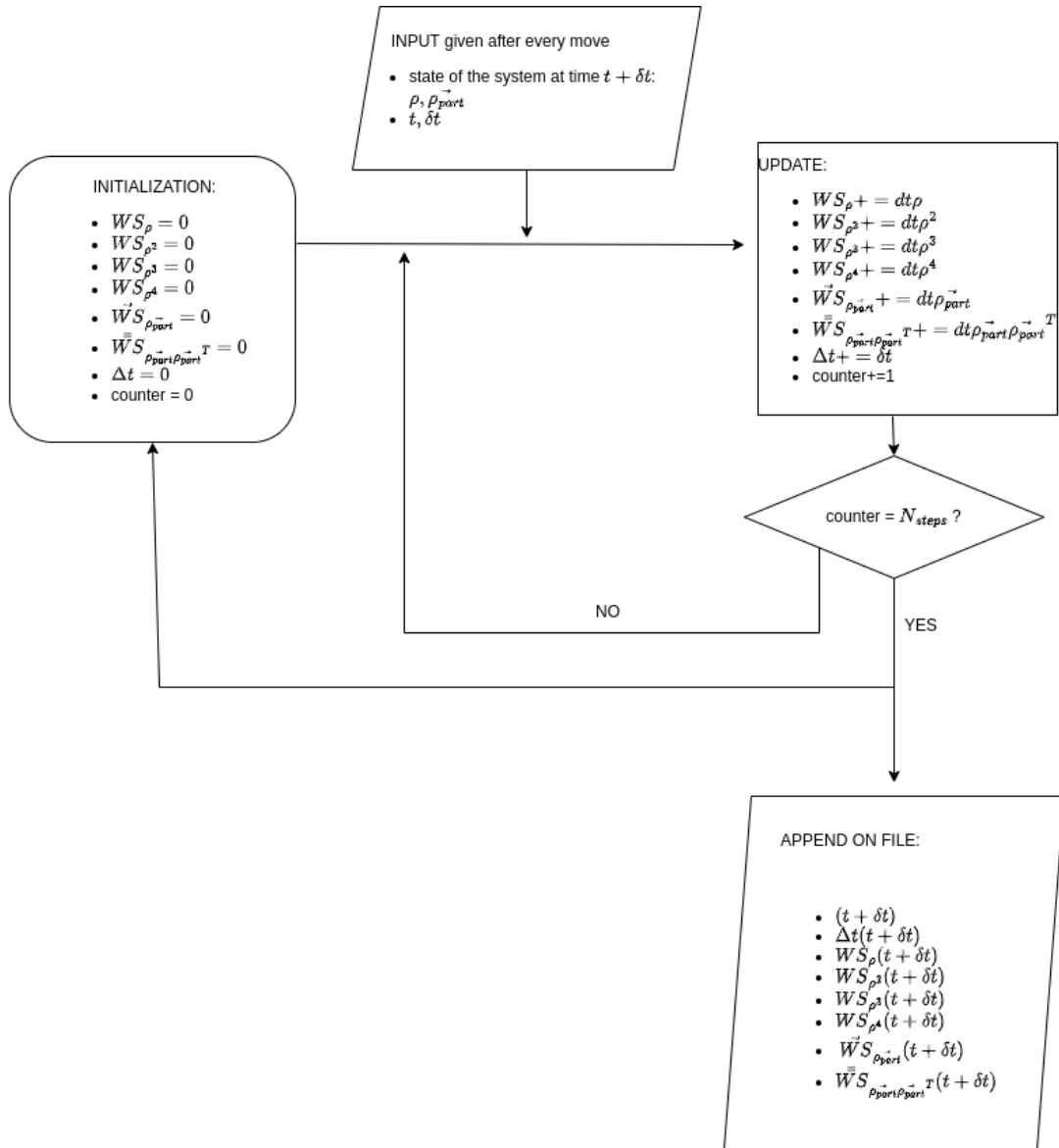


Figure 5.3: Strategy adopted to track statistics during the simulation

Chapter 6

Results

*“Do I wanna know?”
Arctic Monkeys, AM*

As introduced in Sec. 4.3, I studied the stationary state for the following scenarios:

1. $\rho_{B'B} \hat{A} \left| \begin{array}{l} (g, \frac{N_{aux}}{N_{sites}}) \\ \frac{k_{insB}}{k_{diffB}} = 10^{-6} \end{array} \right.$
2. $\rho_{AB} \hat{A} \left| \begin{array}{l} (g, \frac{N_{aux}}{N_{sites}}) \\ \frac{k_{detA}}{k_{diffB}} = 1, \frac{k_{insB}}{k_{diffB}} = 10^{-6} \end{array} \right.$
3. $\rho_{AB} \hat{A} \left| \begin{array}{l} (g, \frac{N_{aux}}{N_{sites}}) \\ \frac{k_{detA}}{k_{diffB}} = 10^2, \frac{k_{insB}}{k_{diffB}} = 10^{-6} \end{array} \right.$

thus obtaining phase diagrams in the $(g, \frac{N_{aux}}{N_{sites}})$ space. As in [22], the sorting process is considered optimal when the mean residence time of the cargo (the time passing from the instant cargo is inserted on the membrane and the instant it is extracted) is minimal. Mean residence time of the cargo is proportional to the density of cargo reached at the stationary state. Differently from [22], in the present case also auxiliary molecules are involved, which are present in a fixed density $\rho_{aux} \sim N_{aux}/N_{sites}$ on the membrane (this is true for B' species and A species in the case of large k_{insA}). Since many biological processes take place on the membrane, it is reasonable to require that at optimal sorting the membrane is not overcrowded with endocytic (auxiliary) molecules: in other words a scenario where small ρ_B is achieved at the expenses of large ρ_{aux} is not optimal. For this reason in the following I will focus both on ρ_B and $\rho = \rho_B + \rho_{aux}$.

As explained in the previous chapter, the trajectory of our system is a Markov

Chain, that can be interpreted as a random walk on the graph of all possible configurations of the system, with link-dependent transition probabilities. It follows that, depending on the graph, it may be possible for the system to stuck in (quasi-)absorbing connected components. Hence, in general, the initial condition is not irrelevant. In order to discuss the existence of low density stationary states here I present the results for simulations ¹ starting from an **empty membrane initial condition**. The issue of initial condition will be further discussed in Sec. 6.8. In the following I first present separately the results for the three different cases investigated, then I focus on peculiar features of the model that can be grasped in general.

6.1 Case 1: B'B dynamics

A qualitative view of the behaviour of the B'B model, simulated setting $k_{\text{insB}} = 10^{-6}$, $k_{\text{diffB}} = 1$, $k_{\text{diffB}'} = 1$, $k_{\text{ext}} = 10^5$, can be found in the phase diagram in Fig. 6.1 where, for each couple $(g, N_{\text{aux}}/N_{\text{sites}})$, I represent snapshots of the system taken after the transitory. A quantitative view of the behaviour of average cargo density can be obtained from the plots in Fig. 6.2a, Fig.6.3a - left and Fig. 6.3b-left. The behaviour of $\rho = \rho_B + \rho_{B'}$ (let us recall that in the case at hand $\rho_{B'} = N_{\text{aux}}/N_{\text{sites}}$) is plotted in Fig. 6.2b, Fig. 6.3a-right, Fig. 6.3b-right. In Fig.6.2c and Fig. 6.2d I plot the values reached at the stationary state by the standard deviation of the cargo density and the total density: the reason why the two plots are equal is that in this regime $\rho_{B'} = N_{\text{aux}}/N_{\text{sites}}$, meaning that only ρ_B contributes to fluctuations

. From the plots we observe that, for a low enough $N_{\text{aux}}/N_{\text{sites}}$ ($N_{\text{aux}}/N_{\text{sites}} \leq \alpha < 1.75 \times 10^{-2}$) no sorting takes place, regardless of g , and the system becomes overcrowded with B particles. For a larger $N_{\text{aux}}/N_{\text{sites}}$, instead, we observe the **emergence of an interval of g where low densities are achieved**. This interval becomes larger as the ratio $N_{\text{aux}}/N_{\text{sites}}$ increases, but the final density achieved at the optimal g , for a fixed value of $N_{\text{aux}}/N_{\text{sites}}$, increases.

For large enough g ($g \geq 10^2$) we see that going from $N_{\text{aux}}/N_{\text{sites}} \sim 0.04225$ to $N_{\text{aux}}/N_{\text{sites}} \sim 0.05625$ the system switches from a high density regime to a regime where the density is consistently smaller, but exhibits larger fluctuations. Such fluctuations are linked to the emergence of **large oscillations**, that are specific of this region (see Fig. 6.2c). Their nature will be discussed in Sec.6.5. Interestingly, a comparison between Fig. 6.2a and Fig.6.2c shows that fluctuations are the smallest in correspondence of the region where minimum densities are found.

¹Computational resources were provided by HPC@POLITO (<http://www.hpc.polito.it>) and BigData@PoliTO Cluster (<https://smartdata.polito.it/computing-facilities/>)

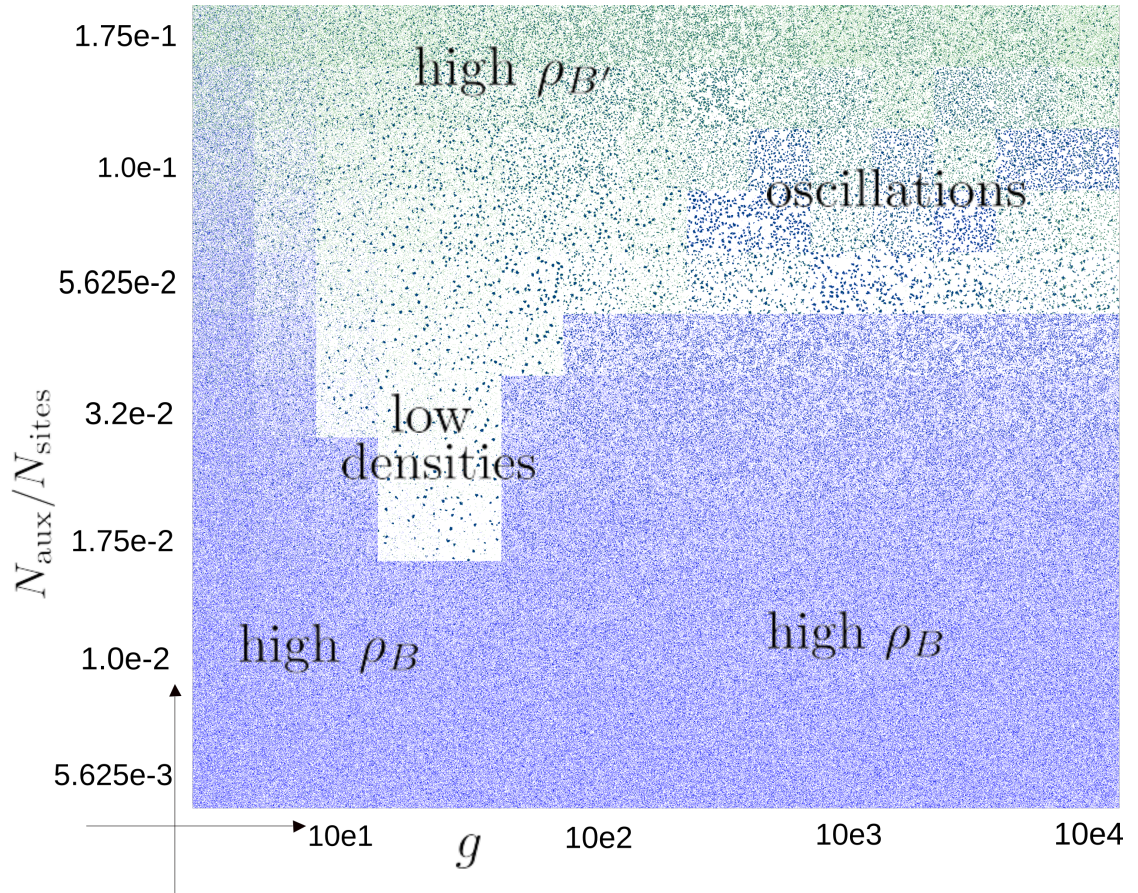


Figure 6.1: Phase diagram for the B'B dynamics

At $N_{\text{aux}}/N_{\text{sites}} = 1.0 \times 10^{-1}$ a **crossover** can be identified: such oscillations decrease in amplitude, ρ_B starts again to decrease, but ρ keeps on increasing. These behaviours are due to the fact that now the system is overcrowded with B' particles, as can also be seen in Fig.6.1.

Fig. 6.4 shows that, for fixed values of g , at optimality, we reach a situation where the quantity of B particles at the stationary state is approximately equal to that of B' particles.

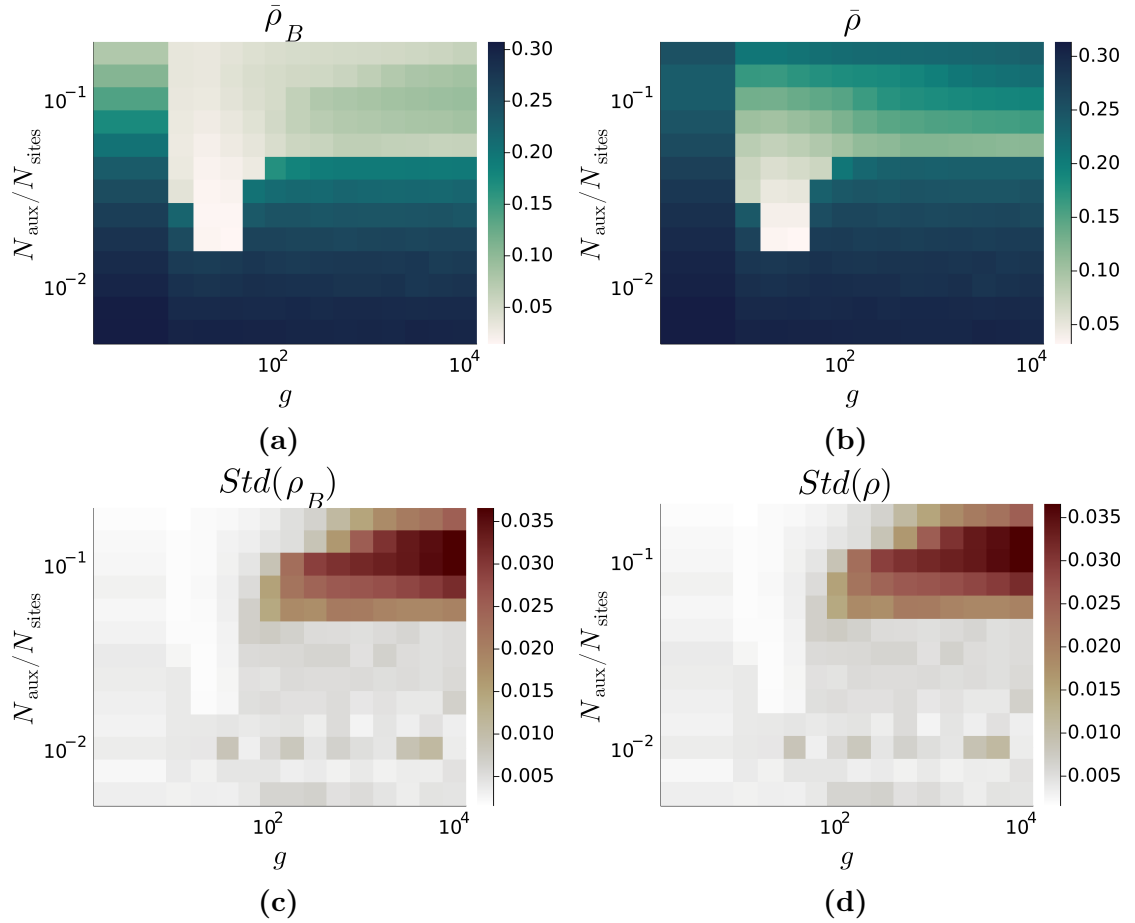


Figure 6.2: B'B dynamics: plots, as a function of $N_{\text{aux}}/N_{\text{sites}}$ and of g , of (a) stationary density of cargo, (b) stationary total density, (c) standard deviation at stationarity of cargo density (d) standard deviation at stationarity of total density.

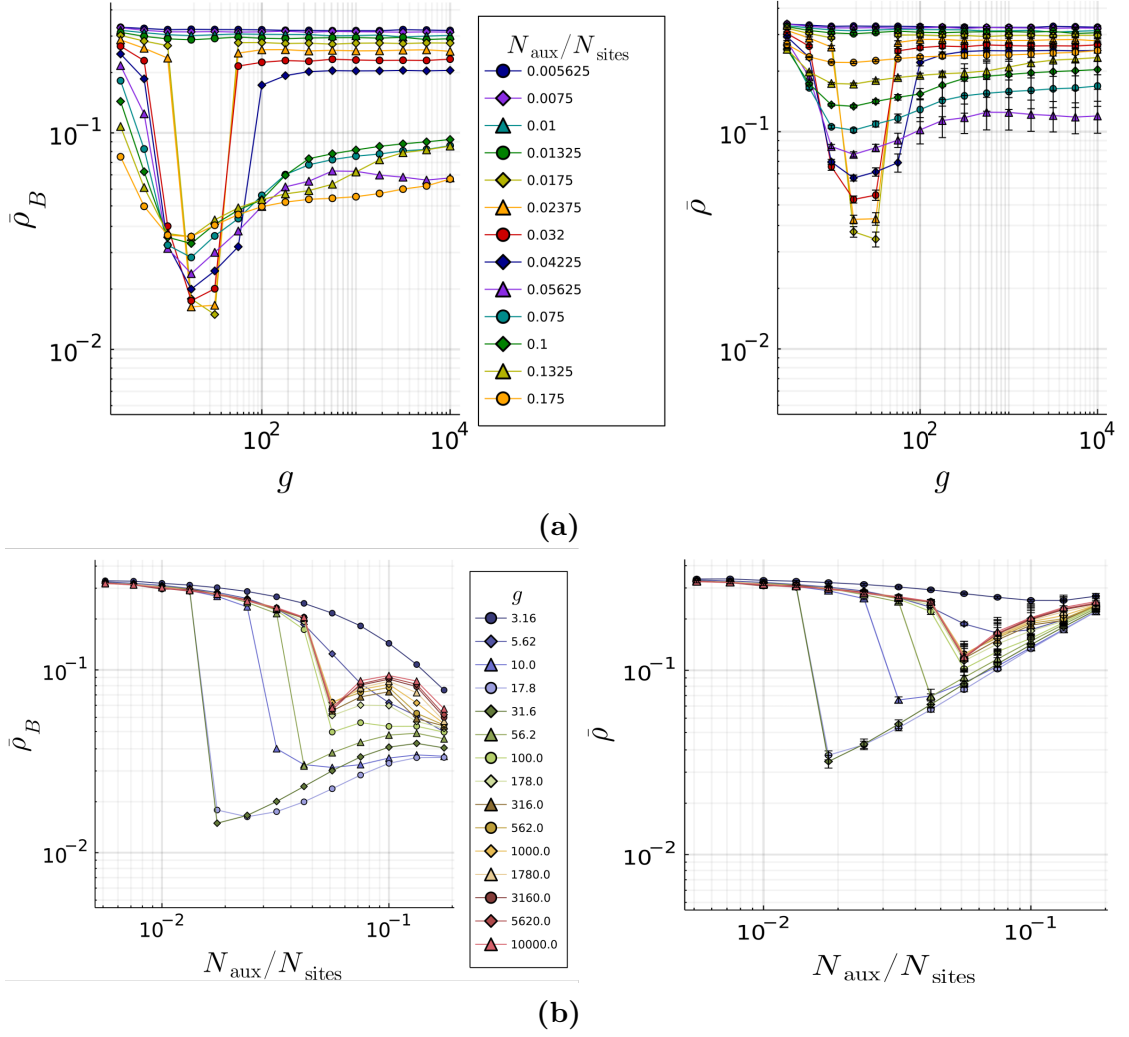


Figure 6.3: B'B dynamics: (a-left) stationary cargo density and (a-right) stationary total density as a function of g ; (b-left) stationary cargo density and (b-right) stationary total density as a function of $N_{\text{aux}}/N_{\text{sites}}$

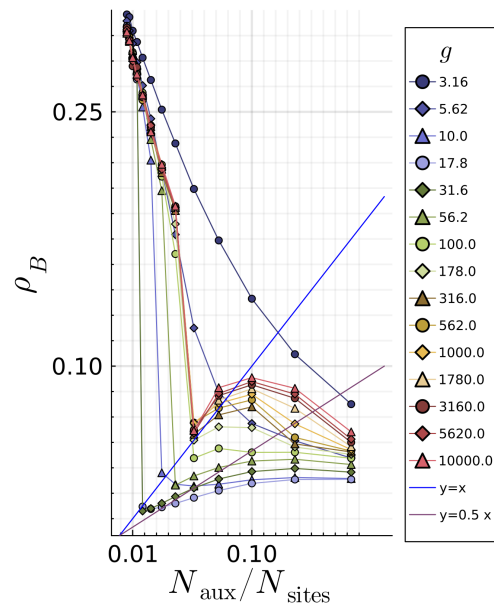


Figure 6.4: B'B dynamics: for fixed g optimal conditions are realized when cargo and auxiliaries are at quasi-equiparity in the stationary state.

6.2 Case 2: AB dynamics

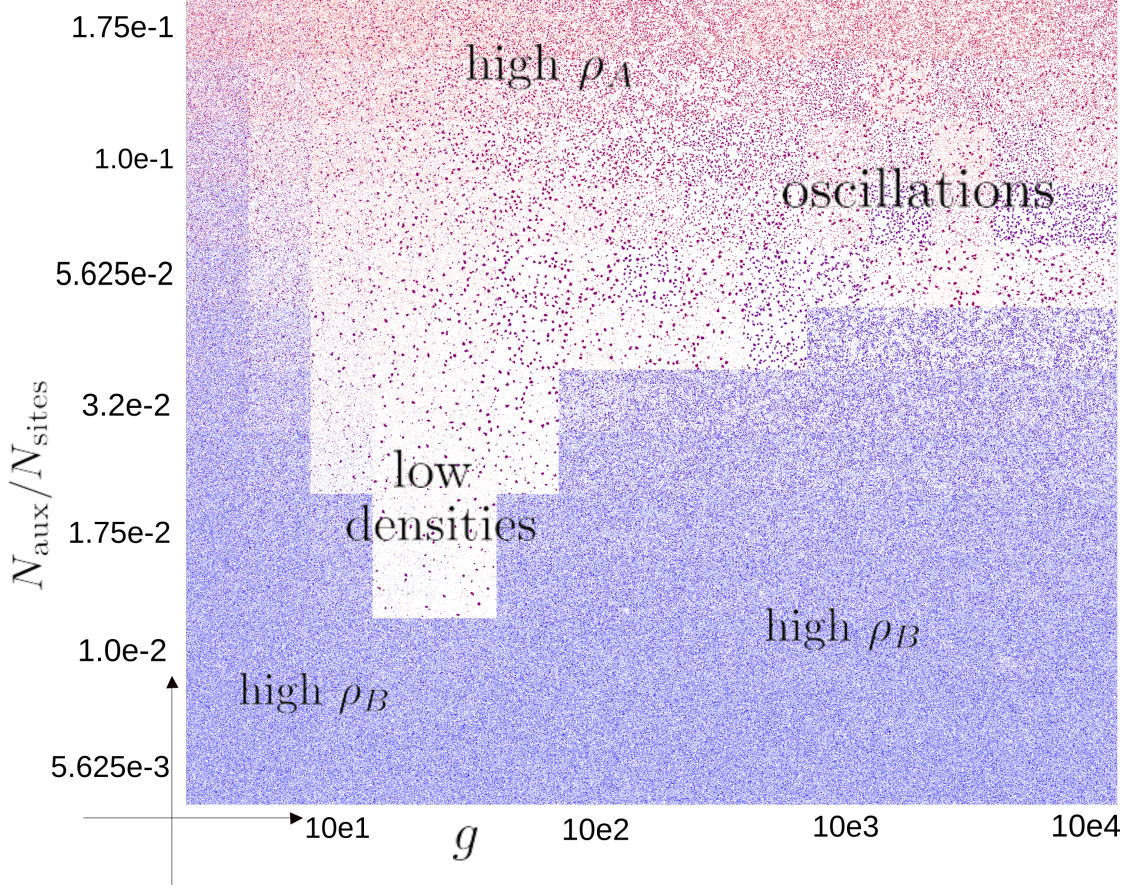


Figure 6.5: Phase diagram for the AB dynamics

A qualitative view of the behaviour of the AB model, simulated setting $k_{\text{insB}} = 10^{-6}$, $k_{\text{diffB}} = 1$, $k_{\text{detA}} = 1$, $k_{\text{insA}} = 10^6$, $k_{\text{ext}} = 10^5$, can be found in the phase diagram in Fig.6.5, which does not differ qualitatively from the previous case (Sec. 6.1). Again, a more quantitative view can be obtained from the plots in Fig. 6.6a and Fig. 6.6b where I plot, respectively, the average density ρ_B and $\rho = \rho_B + \rho_A$ (let us notice that, for large k_{insA} , $\rho_A \simeq N_{\text{aux}}/N_{\text{sites}}$). More details can be seen in Fig.6.7a and Fig.6.7b, while in Fig.6.6c and Fig.6.6d the behaviour of the standard deviation is plotted.

In this case the **appearance of a low density region** is found going from $N_{\text{aux}}/N_{\text{sites}} = 0.01$ to $N_{\text{aux}}/N_{\text{sites}} = 0.01325$. In approximately the same positions as the previous case we see a **large oscillations** region and a **crossover**, where the system becomes overcrowded with A particles.

Fig. 6.8 shows that, for fixed values of g , at optimality, we reach a situation where the quantity of B particles at the stationary state is approximately equal to that of A particles.

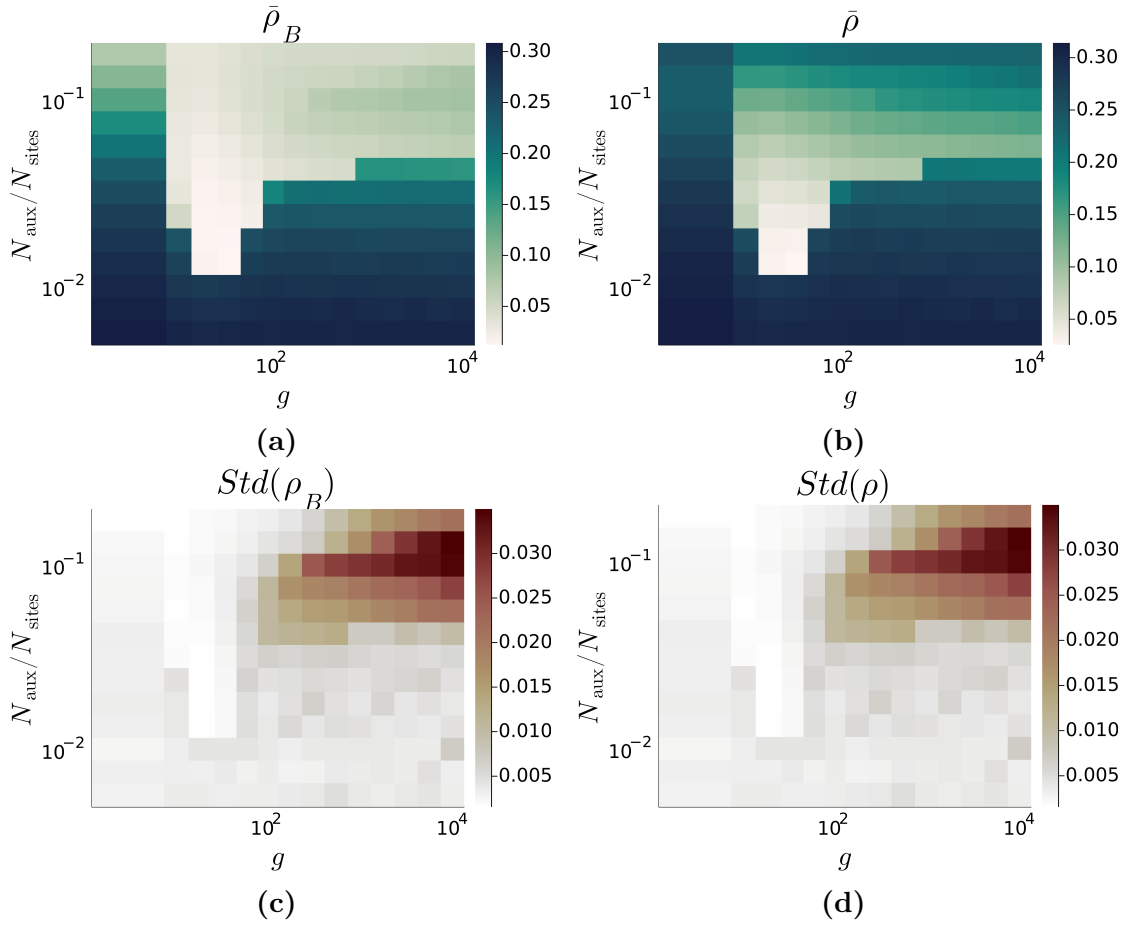


Figure 6.6: AB dynamics: plots, as a function of $N_{\text{aux}}/N_{\text{sites}}$ and of g , of (a) stationary density of cargo, (b) stationary total density, (c) standard deviation at stationarity of cargo density (d) standard deviation at stationarity of total density.

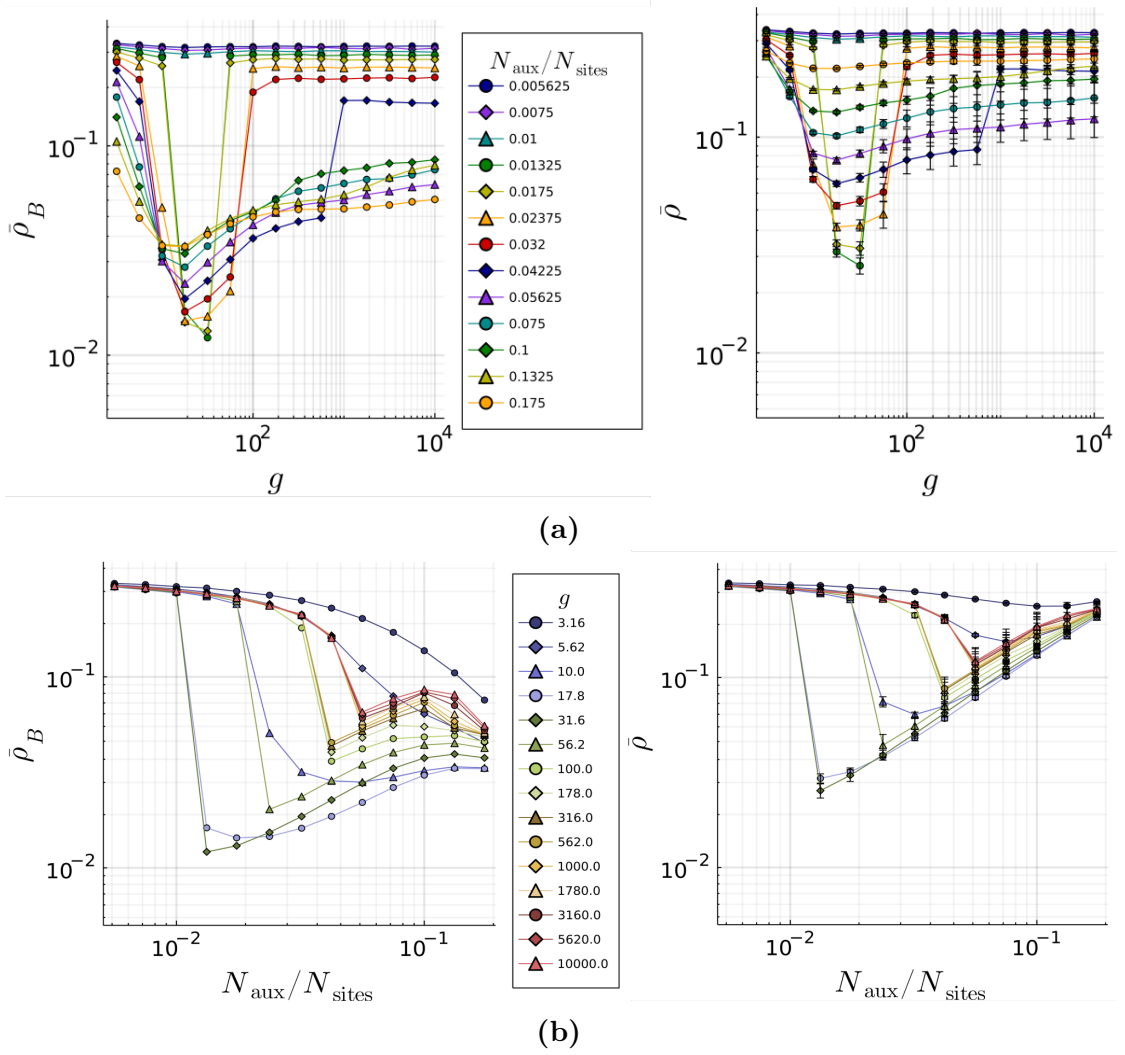


Figure 6.7: AB dynamics: (a-left) stationary cargo density and (a-right) stationary total density as a function of g ; (b-left) stationary cargo density and (b-right) stationary total density as a function of $N_{\text{aux}}/N_{\text{sites}}$

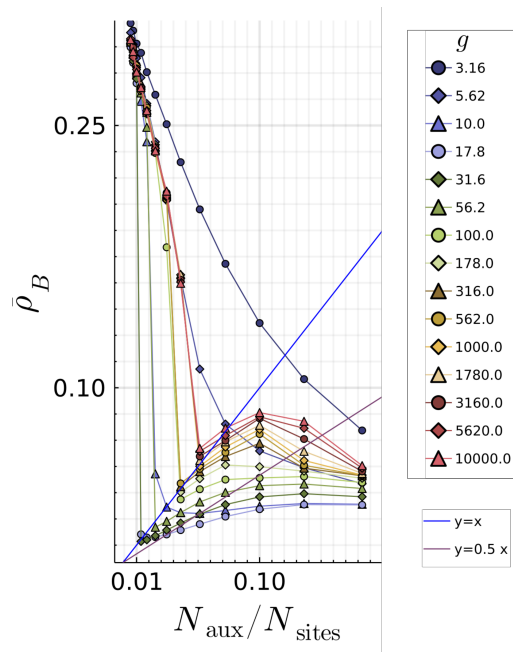


Figure 6.8: AB dynamics: for fixed g optimal conditions are realized when cargo and auxiliaries are at quasi-equipolarity in the stationary state.

6.3 Case 3: fast AB dynamics

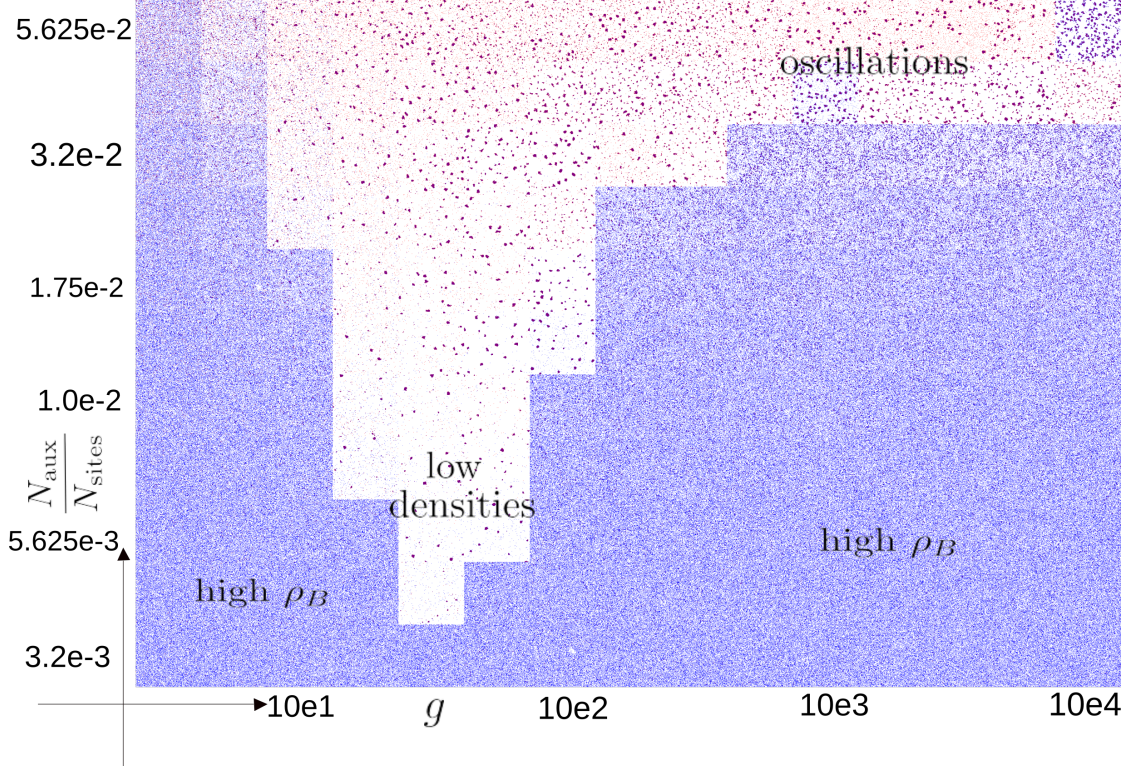


Figure 6.9: Phase diagram for the fast AB dynamics

A qualitative view of the behaviour of the AB model, simulated setting $k_{\text{insB}} = 10^{-6}$, $k_{\text{diffB}} = 1$, $k_{\text{detA}} = 10^2$, $k_{\text{insA}} = 10^8$, $k_{\text{ext}} = 10^5$, (“fast AB dynamics”) can be found in the phase diagram in Fig.6.9. Again it shows a behaviour similar to the previous ones, notice however that it is shifted to lower values of $N_{\text{aux}}/N_{\text{sites}}$. Again, a more quantitative view can be obtained from the plots in Fig. 6.10a, and in Fig. 6.6b where I plot, respectively, the average density ρ_B and $\rho = \rho_B + \rho_A$. More details can be seen in Fig.6.11a,6.11b, 6.12. In Fig.6.10c and Fig.6.10d the behaviour of the standard deviation is plotted.

The **appearance of a low density region** is found for $N_{\text{aux}}/N_{\text{sites}} \geq \alpha$ with $\alpha \in (3.2 \times 10^{-3}, 4.225 \times 10^{-3}]$. The emergence of **large oscillations** is found for $N_{\text{aux}}/N_{\text{sites}} \gtrsim 4.225 \times 10^{-2}$.

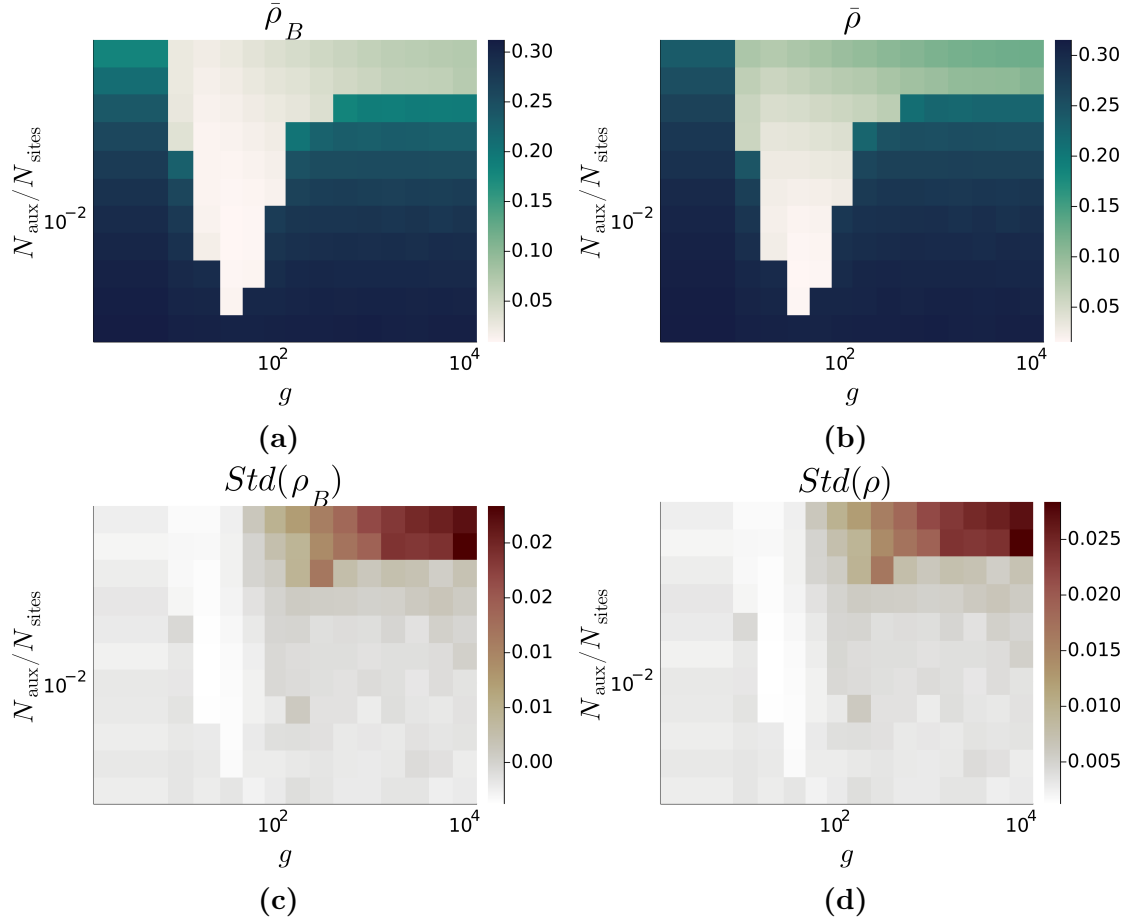


Figure 6.10: fast-AB dynamics: plots, as a function of $N_{\text{aux}}/N_{\text{sites}}$ and of g , of (a) stationary density of cargo, (b) stationary total density, (c) standard deviation at stationarity of cargo density (d) standard deviation at stationarity of total density.

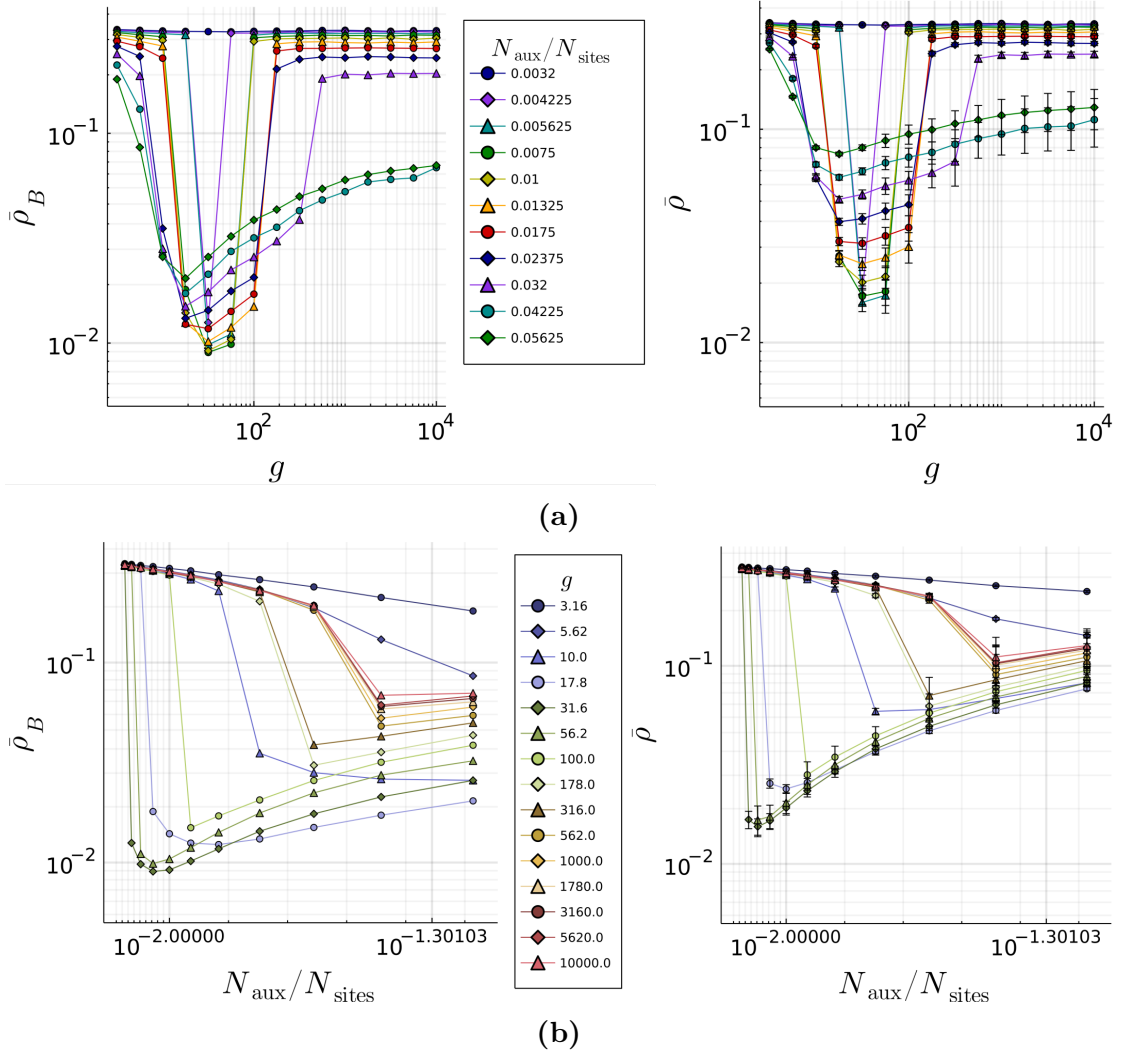


Figure 6.11: fast-AB dynamics: (a-left) stationary cargo density and (a-right) stationary total density as a function of g ; (b-left) stationary cargo density and (b-right) stationary total density as a function of N_{aux}/N_{sites}

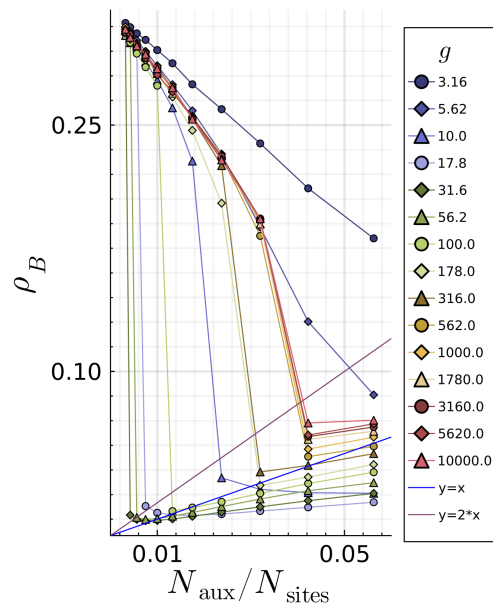


Figure 6.12: AB-fast dynamics: stationary cargo density versus $N_{\text{aux}}/N_{\text{sites}}$ (non-logarithmic scale)

6.4 Comparison between the three cases

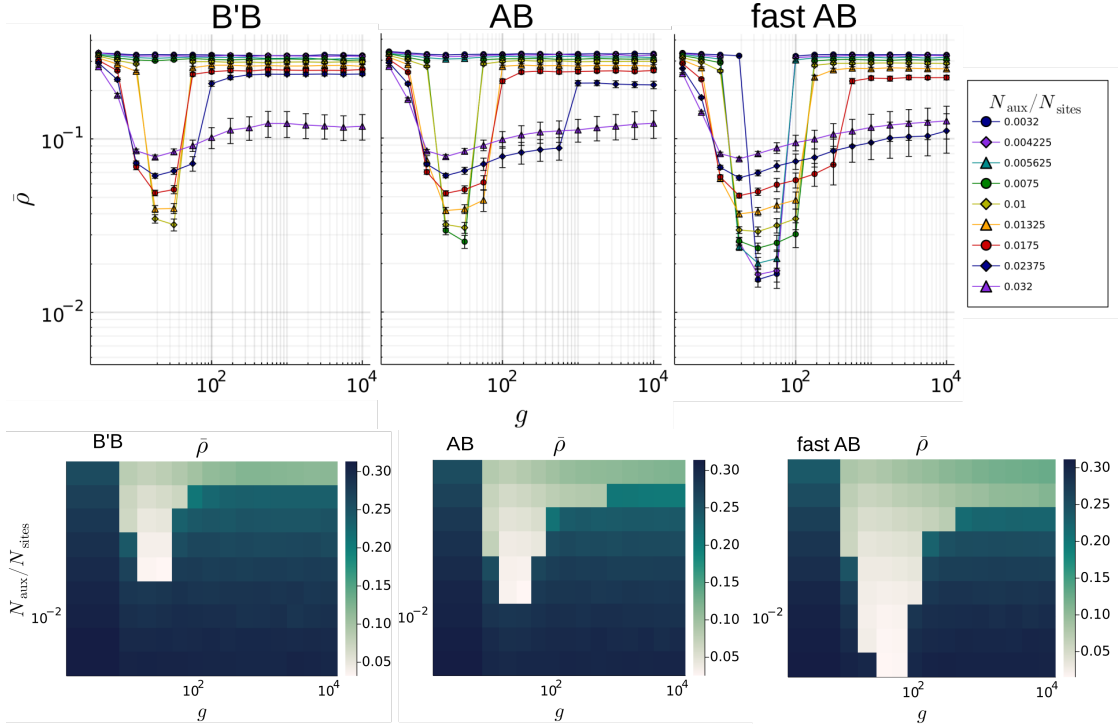


Figure 6.13: Comparison of the behaviour of total density reached at stationary state for the three scenarios investigated. A faster rearrangement mechanism of the auxiliaries enlarges the “sorting region” and allows to reach smaller values of the density.

Fig.6.13 compares the three cases investigated. This comparison suggests that a faster rearrangement mechanism of the auxiliaries enlarges the “sorting region” and allows sorting to take place even for lower values of $N_{\text{aux}}/N_{\text{sites}}$. The region not only gets larger, but also the optimal values of ρ (and of ρ_B) become smaller and are always found at the smallest possible $N_{\text{aux}}/N_{\text{sites}}$ where it is possible to find a low density state.

The role of a fast redistribution of auxiliary molecules can be seen not only if we focus on the stationary state, but also if we look at the time required to reach a low density stationary state starting from a non-empty membrane. As it will be discussed in Sec. 6.8, for fixed g and $N_{\text{aux}}/N_{\text{sites}}$, the time required to reach a low density stationary state can be significantly lower for the AB dynamics than for the B'B dynamics.

These results are not trivial because, in order to form a domain, B particles are necessary and they follow the same dynamics in all the three cases studied,

possibly making the specific dynamics of the auxiliary molecules (whether A, B' or A with fast shuttling) irrelevant. The results achieved suggest that the dynamics followed by the auxiliaries is not irrelevant and can impact on the process.

6.5 Large oscillations

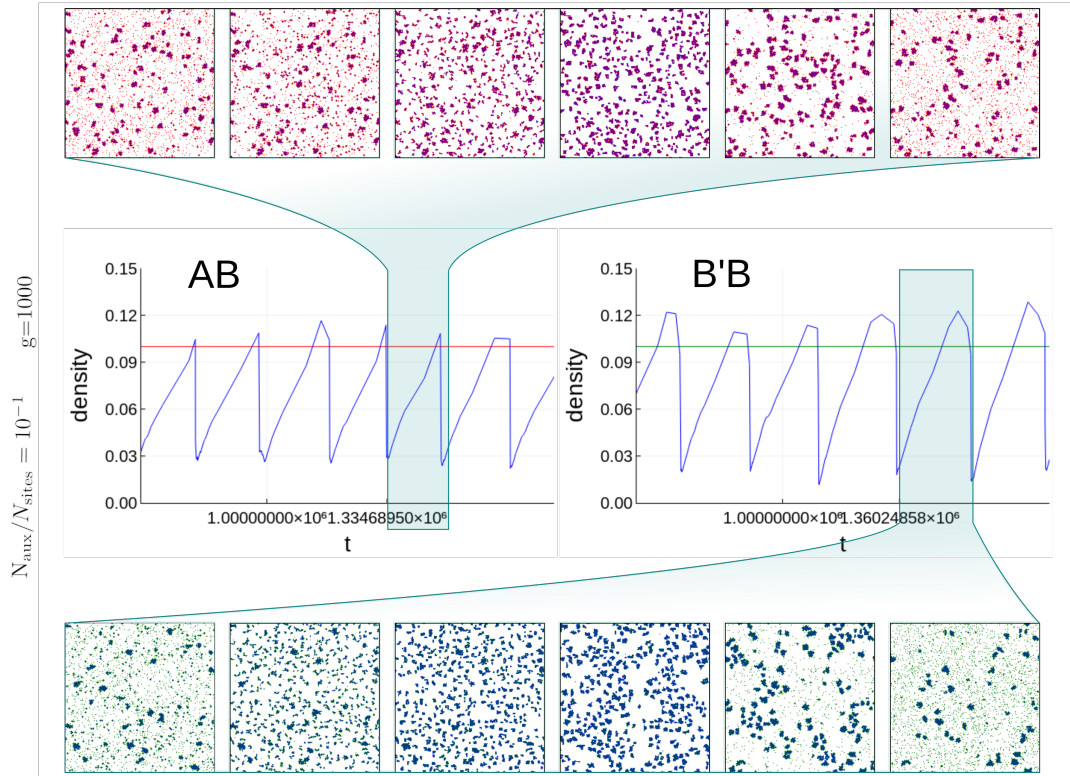


Figure 6.14: Trajectories obtained for the AB and the B'B dynamics and snapshot of the configurations with $N_{\text{aux}}/N_{\text{sites}} = 10^{-1}$ and $g = 1000$. For proper values of the parameters (large-oscillations region), the density of cargo shows large oscillations and the configurations of the system follow a strongly periodic behaviour.

An interesting feature of the two-components model, independently of the specific dynamics followed by the auxiliaries, is the presence of a region where the fluctuations in the density become much larger, as it can be seen from the plots in Fig. 6.2c, Fig.6.6c, Fig.6.10c. Interestingly such larger variance comes with the appearance of relatively regular large oscillations in the density. This feature can be grasped from the example trajectories on the left of Fig. 6.15, that are presented together with their estimated power density spectrum (calculated from

the total density²). A more systematic point of view can be obtained from Fig. 6.16, where for each parameter combination we see the dominant frequency and its power contribution: from these plots we can see that in the large fluctuations region (see again Fig. 6.6c) the evolution of the system is characterized by oscillations of large amplitude (thus large power) and small frequencies.

What's the mechanism behind such oscillations? In Fig.6.14 two example trajectories obtained in this parameter region are represented for the AB and the B'B dynamics, where we see oscillations in ρ_B together with the periodic behaviour of the configurations assumed by the system. Such behaviour is apparently a consequence of having a sufficiently large value of $N_{\text{aux}}/N_{\text{sites}}$, in presence of large values of g : this combination favours the **proliferation of many competing domains** that grow until the totality of auxiliary molecules is depleted. As suggested from the sequence of snapshots in Fig. 6.14, if $N_{\text{aux}}/N_{\text{sites}}$ is sufficiently large it is possible to reach configurations where many domains have a size comparable with the extraction threshold so that, as one domain is extracted, auxiliary molecules are recycled and can successively bind to other domains, allowing them to reach the extraction threshold end being extracted at their time. The result is thus a cascade of extractions. Fig. 6.2c and Fig. 6.6c show that such large oscillations are present only for a *range* of $N_{\text{aux}}/N_{\text{sites}}$. Indeed, if this value is too small the large g causes the auxiliary molecules to remain frozen in small clusters, preventing sorting; on the contrary, for larger $N_{\text{aux}}/N_{\text{sites}}$, we can expect that the auxiliaries cease to be a limiting factor and oscillations decrease in amplitude.

The mechanism just described implies the **periodic alternation** between long “**quiescent**” intervals where extractions are rare events and intervals characterized by **cascades of extractions**. Indeed, this can be seen in the example trajectory in Fig.6.15f. Such regular behaviour cannot be found in other regions. This idea can be assessed more systematically by performing a preliminary analysis on the sequence of the extraction instants (that are recorded during the simulations). In particular it is possible to obtain the time series

$$h(t) = \text{number of extraction events occurred in the interval}[t - \Delta/2, t + \Delta/2)$$

Fig.6.17 (top-right) shows an estimate of its variance, that reaches the highest values in correspondence of the large-oscillations region. Fig.6.17 (left and bottom-right) also shows that in this region low frequencies are important.

²Technical remark: as presented in Ch.5 the simulation algorithm records a value for the density every N steps. The recorded value is a time-weighted average of all the densities assumed in the last N steps, this implies that the obtained signal is smoothed (which is not a great problem since we are interested in smaller frequencies) and non-uniformly sampled. To do the analysis I first linearly interpolated the signal and then estimated the power spectral density by computing the Fourier transform of the auto-correlation function of the signal (Wiener-Khinchin theorem)

A similar analysis can be done also on the time series $f(t)$ defined such that

$$f(t) = \text{time elapsed (at } t \text{) since last extraction event}$$

This time series, in the large-oscillations region, should exhibit higher peaks in correspondence of quiescent intervals and is thus expected to show a quasi-periodic behaviour. This can be confirmed estimating the power density spectrum of the signal (Fig. 6.18).

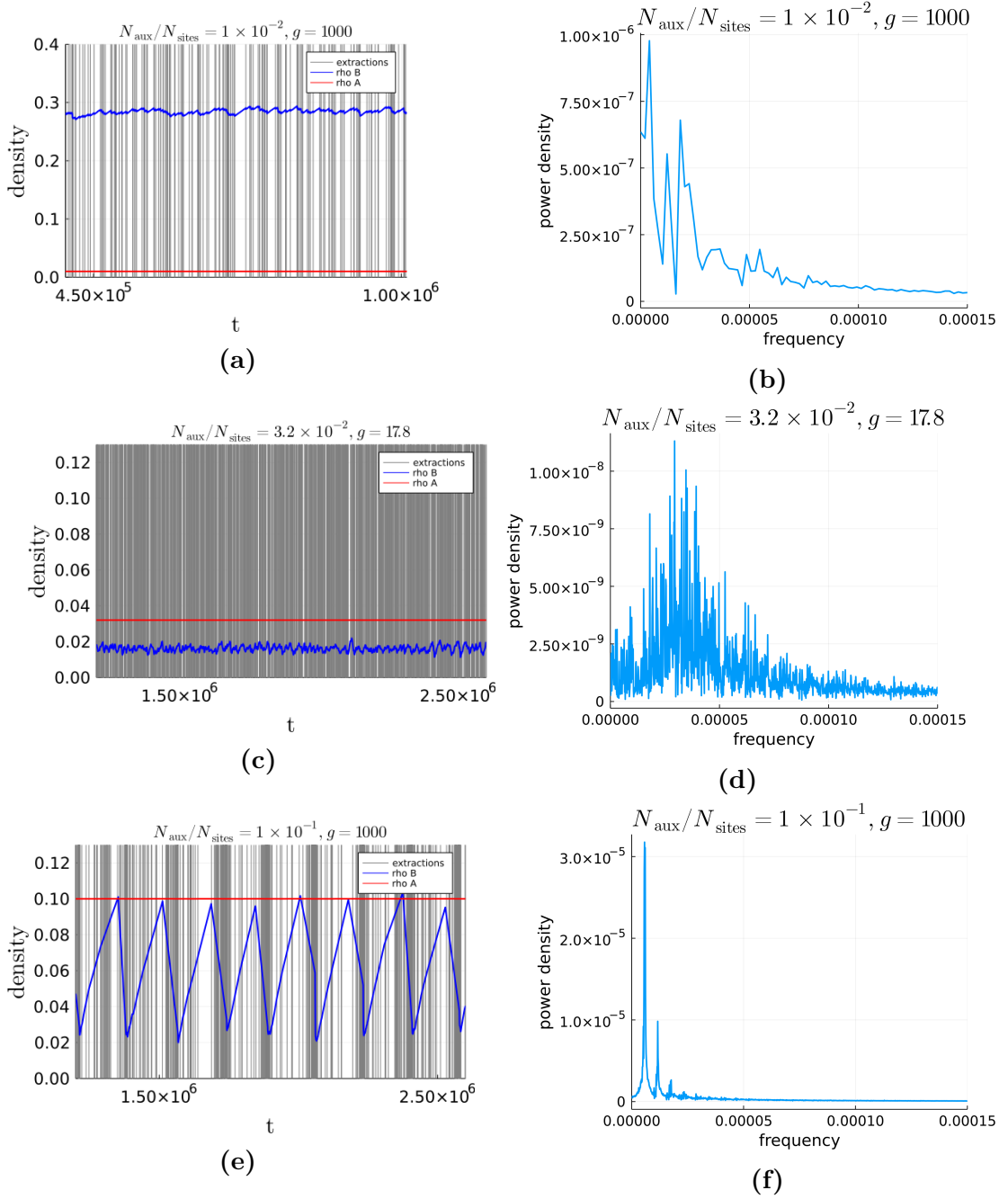


Figure 6.15: Figures on the left represent trajectories obtained for the AB dynamics in different parameter regions (red= ρ_A , blue= ρ_B , vertical bar = extraction event). Figures on the right show the associated power spectra. The third example comes from the large fluctuations region: here we see large oscillations, corresponding to a peak in the spectrum, and the alternation between periods where extractions are very rare and periods of intense extraction activity.

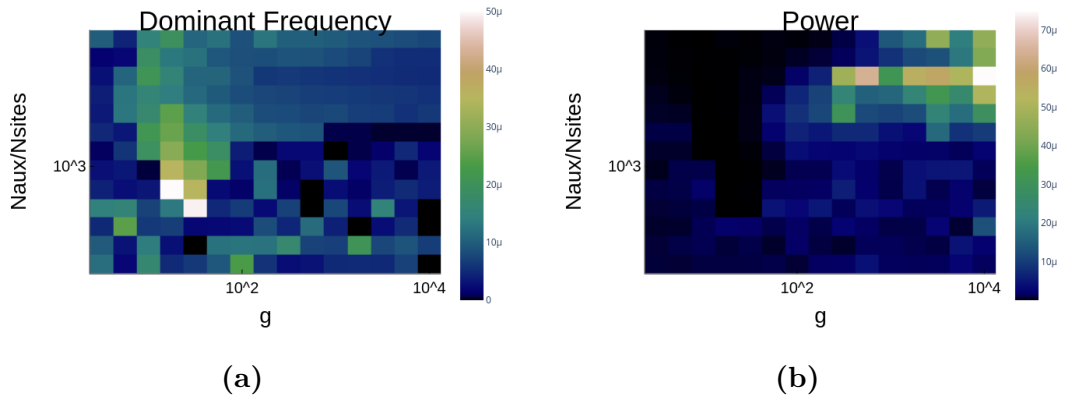


Figure 6.16: Spectral analysis of ρ evolution at stationarity, for the AB case: dominant frequencies (left) and their associated power (right). For large g and large $N_{\text{aux}}/N_{\text{sites}}$ the stationary state is characterized by oscillations of large amplitude (thus large power) and small frequencies. In the region where sorting is disfavored and the system reaches high densities, the plot is more irregular. This is probably due to the fact that here the signal itself is more irregular and, to have a more detailed analysis, the system should be simulated for longer times.

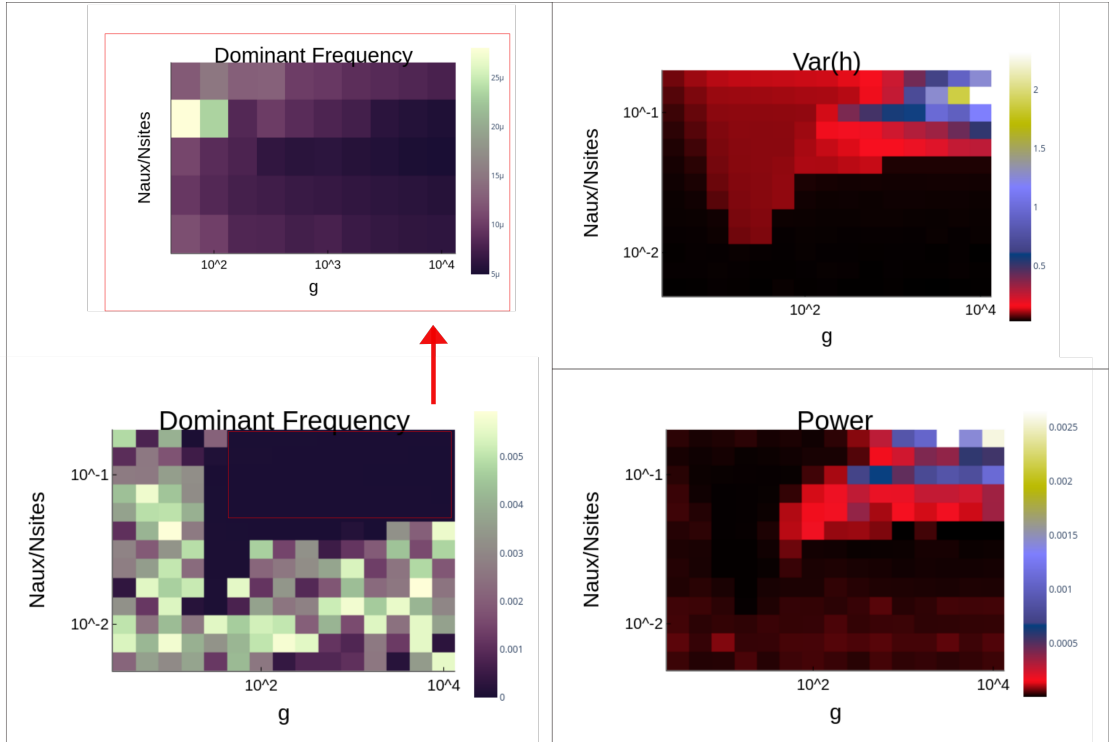


Figure 6.17: Analysis of the signal $h(t)$ ($h(t)$ = number of extraction events occurred in the interval $[t - \Delta/2, t + \Delta/2)$). (top-right) estimated variance. (left) dominant frequencies of the spectrum, with zoom on the top-right region (bottom-right) associated power. These results are compatible with the observation that, in the large-oscillations region, we observe the alternation of long “quiescent” periods (where extractions are more rare) and periods where the extraction activity is more intense. To do the analysis a Δ much smaller than the average time between two extraction events was chosen (in order to obtain a train of spikes).

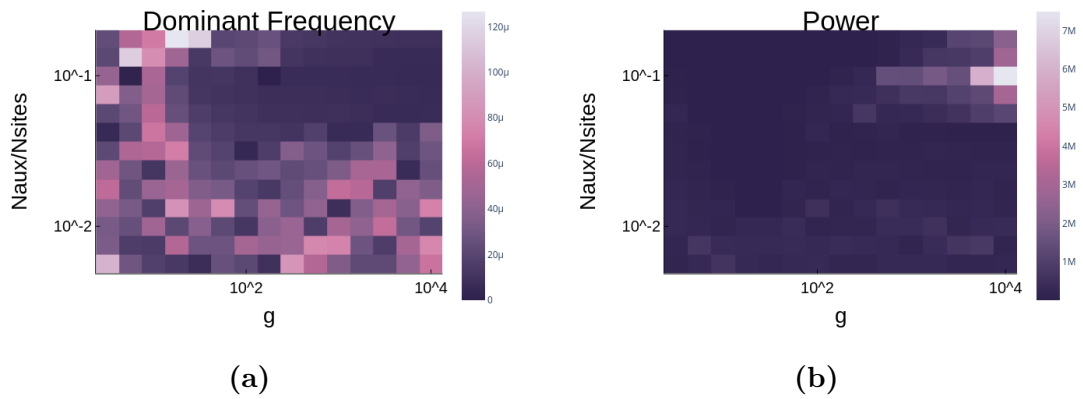


Figure 6.18: Spectral analysis of $f(t)$ ($f(t)$ = time elapsed, at t , since last extraction event) for the AB case: dominant frequencies (left) and their associated power (right). This result is compatible with the observation that, in the large-oscillations region, we observe “quiescent” periods (where long time passes between one extraction and the other) and periods where the extraction activity is more intense. The analysis was performed considering a sampling period much smaller than the average time between two extraction events.

6.6 Comparison with the one-component model

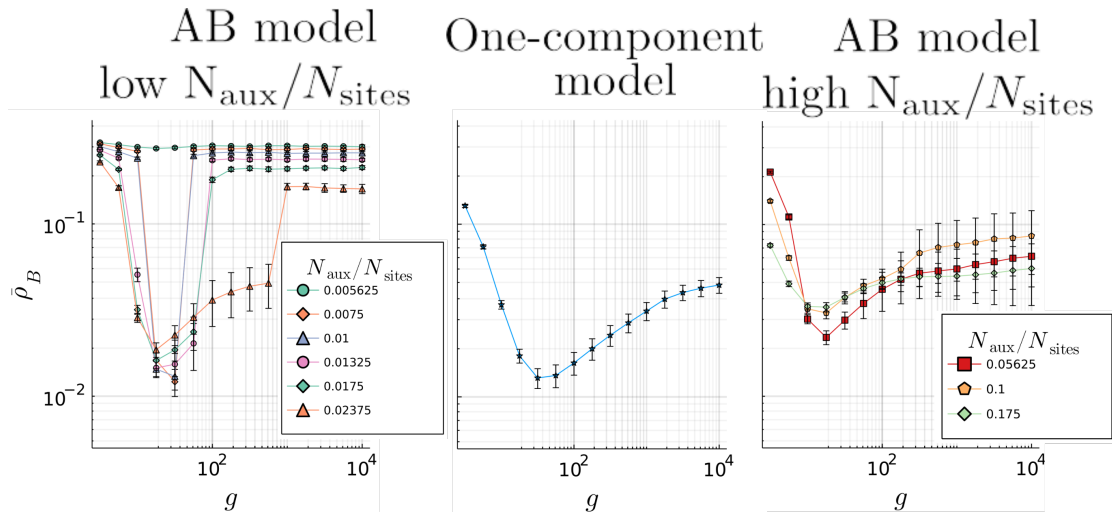


Figure 6.19: Comparison between the one-component model (center) and the AB model (right and left).

Independently from the specific dynamics followed by the auxiliary molecules, a specificity of the two-component model is that a domain requires the presence of both species in order to be stable, but one of them is present in a limited quantity. This apparently simple feature introduces behaviours that are not found in the one-component model studied in [22]. This can be seen in Fig. 6.19, where the behaviour of ρ_B as function of g , in the AB model, is compared to the density behaviour in the one-component model described in [22]. The former is simulated setting that the particles involved have the same insertion rate and diffusion rate of B molecules in the AB model, while the extraction threshold is half the one for the AB model (in this way the number of particles removed within an extraction in the one-component model is approximately equal to the number of B molecules removed during an extraction in the AB model, however a similar curve is obtained setting the same extraction threshold).

From the plots we see that, for large values of $N_{\text{aux}}/N_{\text{sites}}$ (Fig. 6.19, rightmost panel) the behaviour of ρ_B as a function of g is reminiscent of that in the one-component model, with the difference that fluctuations (error bars represent the standard deviation) become larger for increasing values of g : this is because the large-oscillations phenomenon described in Sec.6.5. As $N_{\text{aux}}/N_{\text{sites}}$ decreases, the minimum of ρ_B reaches smaller values and it gradually shifts to larger values of g . It is to notice, however, that the optimal values for g are in approximately the same region as in the one-component model.

For low enough $N_{\text{aux}}/N_{\text{sites}}$ (Fig. 6.19, leftmost panel), **sharp transitions** take place. Indeed it is possible to identify an interval of g where the functional form of $\rho_B(g)$ $\Big|_{N_{\text{aux}}/N_{\text{sites}}}$ is similar to that found at larger $N_{\text{aux}}/N_{\text{sites}}$ while, going out of this interval, sorting is much more disfavoured and high densities are reached. This interval becomes smaller for decreasing $N_{\text{aux}}/N_{\text{sites}}$, until we get a “sorting well” (a small region where sorting takes place and small densities are reached). The origin of such sharp transitions, that are not observed in the one component model, is discussed in Sec. 6.7.

Interestingly, the global minimum for ρ_B in the AB model is approximately the same of the one in the one-component model, but it becomes smaller for a faster rearrangement of A molecules (AB - fast dynamics, see Fig. 6.11a - left) : this allows us to hypothesise that the coupling of cargo with fast auxiliaries may be advantageous with respect to a system where only cargo self-aggregate. This idea would need further investigation.

6.7 Observed transitions

As introduced in the previous sections, the two-component model shows non trivial transitions, independently from the specific dynamic of auxiliaries. Such transitions are schematically represented in Fig. 6.20 for the AB dynamics (same qualitative conclusions should apply also to the other two cases, though): notice that this is no formal classification at all, but just a convenient way to describe the behaviour of the system. In particular we see that, for low $N_{\text{aux}}/N_{\text{sites}}$, **a low density state of the system becomes less stable** when moving away from the optimal g (case (a) and (c)) and as the number of auxiliaries is sufficiently decreased (case (b)). The trajectories plotted suggest that a situation where $\rho_B > \rho_A$ can lead to a destabilization of a low density (not overcrowded with B particles) stationary state. So, when fluctuations in ρ_B become larger, they become able to (irreversibly) disrupt the order maintained by the system, leading to configurations overcrowded with B molecules. Large values of g hinder the ability of auxiliaries to redistribute, thus disfavoured sorting and leading to system overcrowding; however, as $N_{\text{aux}}/N_{\text{sites}}$ increases (case (e)) such a **crowded state becomes less stable** and we enter a large oscillations regime. The same is observed if, for sufficiently large $N_{\text{aux}}/N_{\text{sites}}$, we go from large values of g to smaller ones (case (d)). Such phenomenological observations therefore suggests that the observed abrupt transitions are caused by the fact that **the stability of high density and low density states varies as the parameters change**. It points out also the necessity to investigate long time stability of the stationary states identified. Interestingly, for the parameters where smallest densities are reached, also the fluctuations are the smallest: this supports

the idea that such region may remain stable also for longer times.

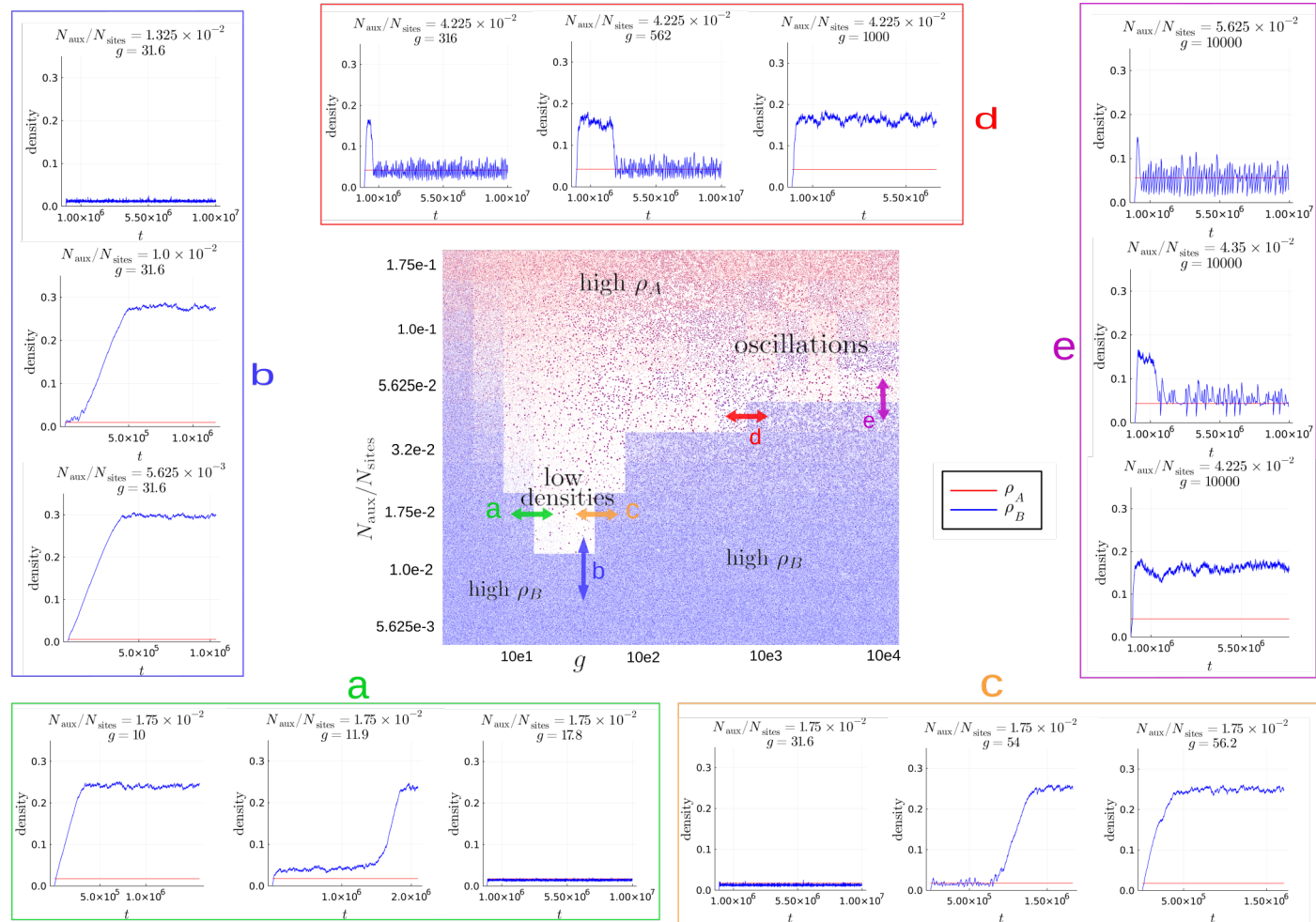


Figure 6.20: Phase diagram for the AB model and trajectories of the system for different values of the parameters, when crossing transitions. As the parameters change, also the long time stability of a low/high density stationary state changes.

6.8 Dependence on the initial conditions

Fig.6.21 and Fig.6.22 show example simulations of the AB and the B'B dynamics starting from $\rho_B(t = 0) = 0.0$ and $\rho_B(t = 0) = 0.10$, for different combinations of $(g, N_{\text{aux}}/N_{\text{sites}})$. We see that in some cases, starting from $\rho_B(t = 0) = 0.10$, can bring the system to a large-density (eventually trapping) state. Auxiliaries following a A dynamics can allow the system to reach low densities faster. So, in general, the initial condition is not irrelevant and, depending on the dynamics of the auxiliaries, the time required to reach low densities may be different. Shuttling mechanism can make the system more robust to variations in the initial condition.

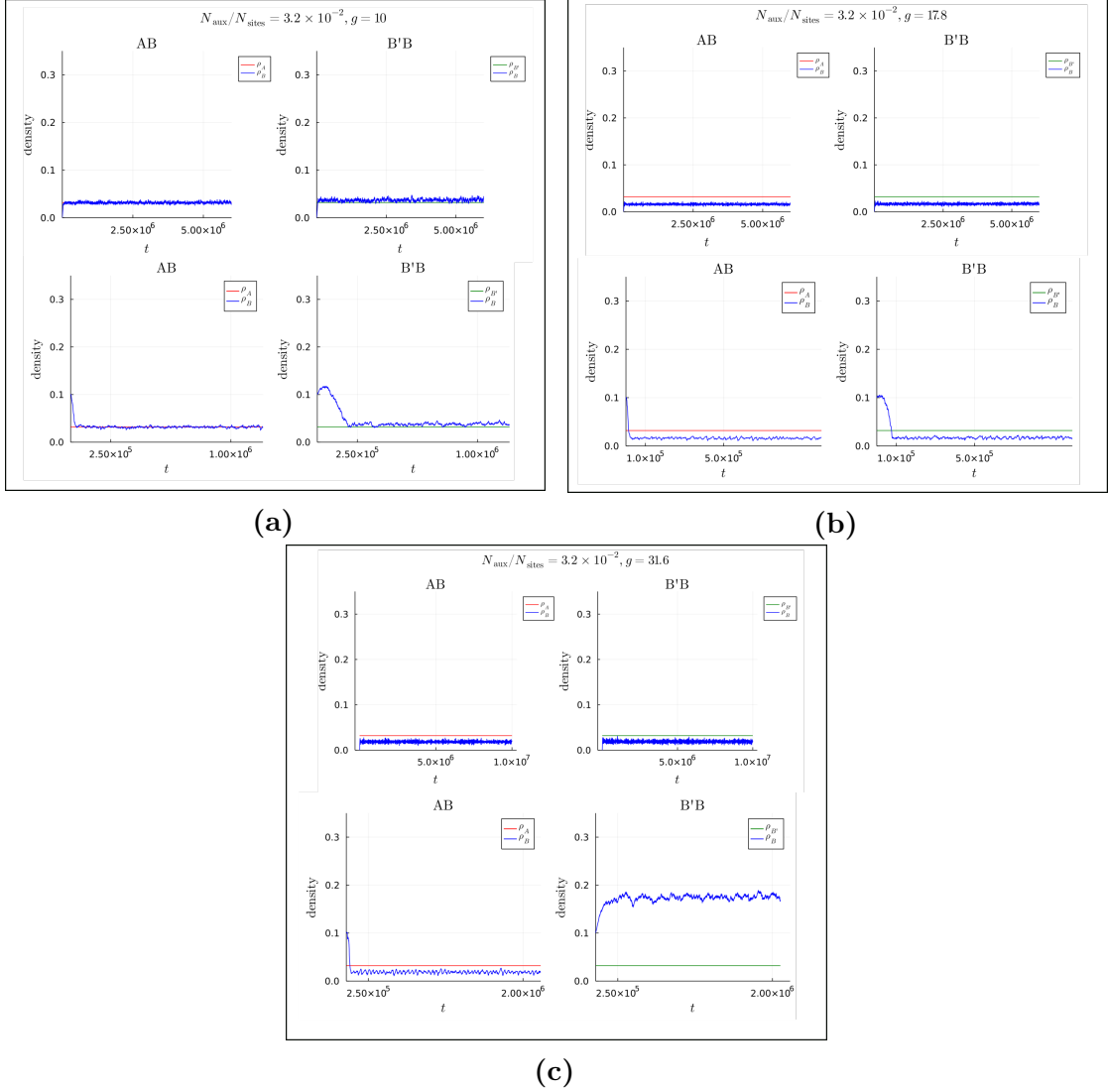


Figure 6.21: Evolution of the system starting from $\rho_B(t=0) = 0.0$ and from $\rho_B(t=0) = 0.10$, for the AB and the B'B dynamics (blue = ρ_B , red = ρ_A , green = $\rho_{B'}$) at $N_{\text{aux}}/N_{\text{sites}} = 3.2 \times 10^{-2}$. Starting from $\rho_B(t=0) = 0.10$, for $g = 10$ and $g = 17.8$ (top-left and top-right) relaxation is faster for the AB dynamics. For $g = 31.6$ (bottom) the B'B dynamics is attracted by a high density (possibly trapping) state.

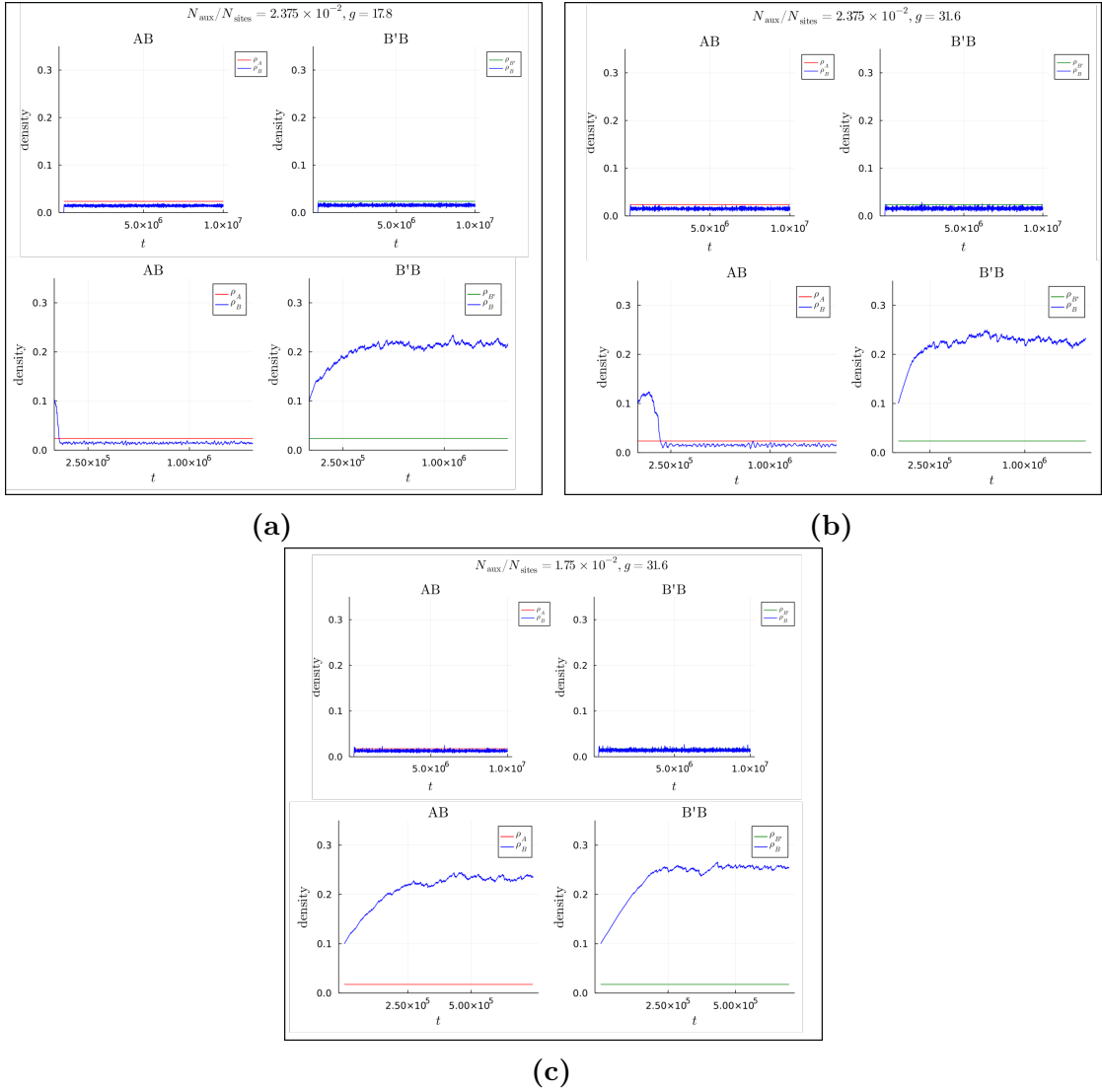


Figure 6.22: Evolution of the system starting from $\rho_B(t=0) = 0.0$ and from $\rho_B(t=0) = 0.10$, for the AB and the B'B dynamics (blue = ρ_B , red = ρ_A , green = $\rho_{B'}$). When starting from $\rho_B(t=0) = 0.10$, for $N_{\text{aux}}/N_{\text{sites}} = 2.375 \times 10^{-2}$, $g = 17.8$ and $g = 31.6$ (top-left and top-right) the B'B dynamics reaches a high density (a longer simulation should reveal whether it ultimately relaxes to a low density stationary state) while the AB dynamics reaches a low density stationary state. For $N_{\text{aux}}/N_{\text{sites}} = 1.75 \times 10^{-2}$ and $g = 31.6$ (bottom) both AB and B'B dynamics reach high densities when starting from $\rho_B(t=0) = 0.10$ (again, longer simulations should reveal whether it ultimately relaxes to a low density stationary state).

Chapter 7

Discussion and conclusions

*“Answers? Questions! Questions? Answers!”
Focus, Focus III*

In this thesis a two-component model for the process of protein sorting was studied, thus extending a previous work [22] that considered only one species (we refer to it as “one-component model”) and describing the interaction of cargo with a pool of auxiliary molecules. Our investigation was driven by two questions:

Q1: How does the quantity of auxiliaries affect the behaviour of the system, considered that auxiliaries are necessary for the formation of sorting domains?

Q2: How can different dynamics of the auxiliaries affect the process?

About question **Q1** we can conclude that a rich phenomenology arises if we study the behaviour of the system varying the number of auxiliaries and the aggregation parameter. In particular, some of these effects appear to come as a consequence of the finiteness of auxiliaries in presence of specific values of the aggregation parameter. First fact to point out is the existence of an optimal region in $(g, N_{\text{aux}}/N_{\text{sites}})$, both for the cargo density and the total density. This is not surprising in that optimality in g is reminiscent of the one-component model, where too small values of g disfavour the formation of sorting domains and too large values of g tend to form many competing domains. The appearance of an optimum also in the quantity of auxiliaries can be explained in a similar fashion. For even larger N_{aux} this effect no more takes place and again we obtain low densities of cargo, which is, however, counterbalanced by an overcrowding with auxiliaries.

If, on the one hand, the existence of an optimal region should not be very surprising, on the other hand it is interesting to notice that the approach to such region is sharp. A reason behind this behaviour apparently stems from the fact that, as we move away from optimal parameters, a low density state of the system becomes more unstable. The instant at which the system destabilizes is reasonably stochastic, highlighting the possible need to further study the long-term stability of

low-density states. The existence of a sharp change in the behaviour of the system, as we vary the parameters, can be interesting from a biological point of view, as it may be linked to switch-like behaviours, which are typical of living cells. However it may be also be an unwanted effect. It should thus be investigated whether this behaviour is actually realized in cells.

In general, the issue of stability appears to be quite relevant in this model, in that it is possible for the system to get stuck in high density (quasi-)stationary states. This implies also that initial conditions can be important.

The finite quantity of auxiliaries is also at the basis of the periodic alternation of intense extraction activity and quiescent periods, a phenomenon that takes place for large g and $N_{\text{aux}}/N_{\text{sites}}$ and results in large oscillations, in time, of the density. Again, this behaviour is not contemplated by the one-component model of [22] and it may be interesting to investigate whether it is found in actual biological system.

Interestingly, switch-like and oscillatory behaviours in vesicle secretion have been theoretically hypothesised [36] following a different approach. They therefore deserve further study, integrating the different theories, as well as experiments.

About question **Q2** we can conclude that a faster shuttling of the auxiliaries can actually bring advantages to the process, allowing sorting to take place even for smaller quantities of auxiliary molecules (for proper values of the aggregation parameter). A faster redistribution process seems also to make the system more robust with respect to variations of the initial conditions and variations in the density of cargo. Results also suggest that a cargo-checkpoint mechanism characterized by a large selectivity of auxiliaries for cargo can increase the efficiency of the process: in facts fast shuttling, in our framework, implies that auxiliary molecules are very prone to leave the membrane in absence of cargo and find another membrane site.

Bibliography

- [1] Erwin Schrodinger. *What is Life?: The Physical Aspect of the Living Cell ; with, Mind and Matter ; & Autobiographical Sketches*. Cambridge University Press, 2012 (cit. on p. 1).
- [2] Encyclopaedia Britannica. *eukaryotic cell*. URL: <https://www.britannica.com/science/cell-biology#/media/1/101396/112877> (cit. on p. 2).
- [3] Encyclopaedia Britannica. *molecular view of the cell membrane*. URL: <https://www.britannica.com/science/cell-membrane#/media/1/463558/45550> (cit. on p. 2).
- [4] Clifford P Brangwynne, Christian R Eckmann, David S Courson, Agata Rybarska, Carsten Hoegel, Jöbin Gharakhani, Frank Jülicher, and Anthony A Hyman. «Germline P Granules Are Liquid Droplets That Localize by Controlled Dissolution/Condensation». In: *Science* 324.5935 (2009), pp. 1729–1732. DOI: 10.1126/science.1172046. URL: <https://www.science.org/doi/abs/10.1126/science.1172046> (cit. on pp. 1, 2).
- [5] Anthony A Hyman, Christoph A Weber, and Frank Jülicher. «Liquid-Liquid Phase Separation in Biology». In: *Annual Review of Cell and Developmental Biology* 30.1 (2014), pp. 39–58. DOI: 10.1146/annurev-cellbio-100913-013325. URL: <https://doi.org/10.1146/annurev-cellbio-100913-013325> (cit. on p. 1).
- [6] Marco Zamparo, F Chianale, Claudio Tebaldi, M Cosentino-Lagomarsino, M Nicodemi, and A Gamba. «Dynamic membrane patterning, signal localization and polarity in living cells». In: *Soft Matter* 11.5 (2015), pp. 838–849 (cit. on p. 1).
- [7] Andrea Gamba, Antonio De Candia, Stefano Di Talia, Antonio Coniglio, Federico Bussolino, and Guido Serini. «Diffusion-limited phase separation in eukaryotic chemotaxis». In: (2005). URL: www.pnas.org/cgi/doi/10.1073/pnas.0503974102 (cit. on p. 1).

- [8] A. Gamba, I. Kolokolov, V. Lebedev, and G. Ortenzi. «Patch coalescence as a mechanism for eukaryotic directional sensing». In: *Physical Review Letters* 99.15 (2007), pp. 1–4. ISSN: 00319007. DOI: 10.1103/PhysRevLett.99.158101 (cit. on pp. 1, 18).
- [9] T. Ferraro, A. De Candia, A. Gamba, and A. Coniglio. «Spatial signal amplification in cell biology: A lattice-gas model for self-tuned phase ordering». In: *Epl* 83.5 (2008). ISSN: 02955075. DOI: 10.1209/0295-5075/83/50009. arXiv: arXiv:0711.3090v1 (cit. on p. 1).
- [10] Matteo Semplice, Andrea Veglio, Giovanni Naldi, Guido Serini, and Andrea Gamba. «A Bistable Model of Cell Polarity». In: *PLOS ONE* 7.2 (2012), pp. 1–14. DOI: 10.1371/journal.pone.0030977. URL: <https://doi.org/10.1371/journal.pone.0030977> (cit. on p. 1).
- [11] Mattia Conte, Luca Fiorillo, Simona Bianco, Andrea M Chiariello, Andrea Esposito, and Mario Nicodemi. «Polymer physics indicates chromatin folding variability across single-cells results from state degeneracy in phase separation». In: *Nature communications* 11.1 (2020), pp. 1–13 (cit. on p. 1).
- [12] Elisa Floris, Andrea Piras, Luca Dall’Asta, Andrea Gamba, Emilio Hirsch, and Carlo C Campa. «Physics of compartmentalization: How phase separation and signaling shape membrane and organelle identity». In: *Computational and Structural Biotechnology Journal* 19 (2021), pp. 3225–3233. ISSN: 2001-0370. DOI: <https://doi.org/10.1016/j.csbj.2021.05.029>. URL: <https://www.sciencedirect.com/science/article/pii/S2001037021002105> (cit. on p. 1).
- [13] Felix Spira, Nikola S Mueller, Gisela Beck, Philipp Von Olshausen, Joachim Beig, and Roland Wedlich-Söldner. «Patchwork organization of the yeast plasma membrane into numerous coexisting domains». In: *Nature cell biology* 14.6 (2012), pp. 640–648 (cit. on p. 2).
- [14] Michael R Speicher and Nigel P Carter. «The new cytogenetics: blurring the boundaries with molecular biology». In: *Nature reviews genetics* 6.10 (2005), pp. 782–792 (cit. on p. 2).
- [15] Alberts et al. *Molecular Biology of the Cell*. Ed. by Garland Science. Garland Science, 2015 (cit. on pp. 3, 4, 8, 28).
- [16] Marko Kaksonen and Aurélien Roux. «Mechanisms of clathrin-mediated endocytosis». In: *Nature Reviews Molecular Cell Biology* 19.5 (May 2018), pp. 313–326. ISSN: 1471-0072. DOI: 10.1038/nrm.2017.132. URL: www.nature.com/nrm%20http://www.nature.com/articles/nrm.2017.132 (cit. on pp. 4–6).

- [17] Li Ma et al. «Transient Fcho12 Eps15R AP2 nanoclusters prime the AP2 clathrin adaptor for cargo binding». In: *Developmental cell* 37.5 (2016), pp. 428–443 (cit. on p. 5).
- [18] Alexander Fotin, Yifan Cheng, Piotr Sliz, Nikolaus Grigorieff, Stephen C Harrison, Tomas Kirchhausen, and Thomas Walz. «Molecular model for a complete clathrin lattice from electron cryomicroscopy». In: *Nature* 432.7017 (2004), pp. 573–579 (cit. on p. 5).
- [19] John E Heuser and RG Anderson. «Hypertonic media inhibit receptor-mediated endocytosis by blocking clathrin-coated pit formation.» In: *The Journal of cell biology* 108.2 (1989), pp. 389–400 (cit. on p. 5).
- [20] Marcelo Ehrlich, Werner Boll, Antoine Van Oijen, Ramesh Hariharan, Kartik Chandran, Max L Nibert, and Tomas Kirchhausen. «Endocytosis by random initiation and stabilization of clathrin-coated pits». In: *Cell* 118.5 (2004), pp. 591–605 (cit. on pp. 6, 7).
- [21] Yan Chen, Jeffery Yong, Antonio Martínez-Sánchez, Yang Yang, Yumei Wu, Pietro De Camilli, Rubén Fernández-Busnadiego, and Min Wu. «Dynamic instability of clathrin assembly provides proofreading control for endocytosis». In: *Journal of Cell Biology* 218.10 (2019), pp. 3200–3211 (cit. on p. 6).
- [22] Marco Zamparo, Donatella Valdembri, Guido Serini, Igor V. Kolokolov, Vladimir V. Lebedev, Luca Dall’Asta, and Andrea Gamba. «Optimality in Self-Organized Molecular Sorting». In: *Phys. Rev. Lett.* 126 (8 Feb. 2021), p. 088101. DOI: 10.1103/PhysRevLett.126.088101. URL: <https://link.aps.org/doi/10.1103/PhysRevLett.126.088101> (cit. on pp. 7, 20, 22, 24–26, 28, 38, 60, 67, 68).
- [23] Elisa Floris et al. *Phase separation and critical size in molecular sorting*. 2022. DOI: 10.48550/ARXIV.2205.03337. URL: <https://arxiv.org/abs/2205.03337> (cit. on pp. 7, 20).
- [24] Joel Berry, Clifford P Brangwynne, and Mikko Haataja. «Physical principles of intracellular organization via active and passive phase transitions». In: *Reports on Progress in Physics* 81.4 (Feb. 2018), p. 46601. DOI: 10.1088/1361-6633/aaa61e. URL: <https://doi.org/10.1088/1361-6633/aaa61e> (cit. on pp. 9, 10, 14).
- [25] P. C. Hohenberg and B. I. Halperin. «Theory of dynamic critical phenomena». In: *Rev. Mod. Phys.* 49 (3 July 1977), pp. 435–479. DOI: 10.1103/RevModPhys.49.435. URL: <https://link.aps.org/doi/10.1103/RevModPhys.49.435> (cit. on pp. 12, 26).
- [26] Roy J Glauber. «Time-dependent statistics of the Ising model». In: *Journal of mathematical physics* 4.2 (1963), pp. 294–307 (cit. on p. 12).

- [27] Kyozi Kawasaki. «Diffusion constants near the critical point for time-dependent Ising models. I». In: *Physical Review* 145.1 (1966), p. 224 (cit. on p. 12).
- [28] Luca Dall’Asta. «Kinetics of phase transitions». In: *Kinetics of Phase Transitions* (2009), pp. 1–61. DOI: 10.1201/9781420008364 (cit. on pp. 13, 14).
- [29] Pavel L. Krapivsky, Sidney Redner, and Eli Ben-Naim. *A Kinetic View of Statistical Physics*. Cambridge University Press, 2010. DOI: 10.1017/CB09780511780516 (cit. on pp. 13, 15, 16, 18, 20).
- [30] Roberto Livi and Paolo Politi. *Nonequilibrium statistical physics: A modern perspective*. 2017, pp. 1–420. ISBN: 9781107278974. DOI: 10.1017/9781107278974 (cit. on pp. 15, 18).
- [31] I M Lifshitz and V V Slyozov. «The kinetics of precipitation from supersaturated solid solutions». In: *Journal of Physics and Chemistry of Solids* 19.1 (1961), pp. 35–50. ISSN: 0022-3697. DOI: [https://doi.org/10.1016/0022-3697\(61\)90054-3](https://doi.org/10.1016/0022-3697(61)90054-3). URL: <https://www.sciencedirect.com/science/article/pii/0022369761900543> (cit. on p. 16).
- [32] Jeferson J. Arenzon, Alan J. Bray, Leticia F. Cugliandolo, and Alberto Sicilia. «Exact Results for Curvature-Driven Coarsening in Two Dimensions». In: *Phys. Rev. Lett.* 98 (14 Apr. 2007), p. 145701. DOI: 10.1103/PhysRevLett.98.145701. URL: <https://link.aps.org/doi/10.1103/PhysRevLett.98.145701> (cit. on p. 18).
- [33] A Gamba, I Kolokolov, V Lebedev, and G Ortenzi. «Universal features of cell polarization processes». In: *J. Stat. Mech* (2009), p. 2019. DOI: 10.1088/1742-5468/2009/02/P02019 (cit. on pp. 18, 19).
- [34] Marco Zamparo, Luca Dall’Asta, and Andrea Gamba. «On the Mean Residence Time in Stochastic Lattice-Gas Models». In: *Journal of Statistical Physics* 174.1 (2019), pp. 120–134 (cit. on p. 21).
- [35] Daniel T Gillespie. «Exact stochastic simulation of coupled chemical reactions». In: *The journal of physical chemistry* 81.25 (1977), pp. 2340–2361 (cit. on p. 31).
- [36] Lionel Foret and Pierre Sens. «Kinetic regulation of coated vesicle secretion». In: *Proceedings of the National Academy of Sciences* 105.39 (2008), pp. 14763–14768 (cit. on p. 68).